Stony Brook University

Study on improvement of plasma etch resistance of photo resists and e-beam resists by sequential infiltration synthesis

A Thesis Presented

by

Xianghai Meng

to

The Graduate School

in Partial Fulfillment of the

Requirements

for the Degree of

Master of Science

in

Materials Science and Engineering

Stony Brook University

May/2013

Stony Brook University

The Graduate School

Xianghai Meng

We, the thesis committee for the above candidate for the

Master of Science degree, hereby recommend

acceptance of this thesis.

Ming Lu – Thesis Advisor
Scientist, Center for Functional Nanomaterials, Brookhaven National Laboratory

Yizhi Meng – Second Reader
Assistant Professor, Materials Science and Engineering

T. A. Venkatesh – Third Reader
Assistant Professor, Materials Science and Engineering

This thesis is accepted by the Graduate School

Charles Taber
Interim Dean of the Graduate School

Abstract of the Thesis

Study on improvement of the plasma etch resistance of photo resists and e-beam resists by sequential infiltration synthesis

by

Xianghai Meng

Master of Science

in

Materials Science and Engineering

Stony Brook University

2013

Deep etch is always a challenge in semiconductor industry due to the requirement of high selectivity and fidelity for the process. Atomic layer deposition (ALD) is a new thin film deposition technique which is self-limiting and provides excellent conformality and reproducibility. Other than the application of deposition, ALD also provides an approach which operates at semi-static mode to modify the characteristic of the bulk of resist, which will render a high resistance to plasma etch as well as sidewall protection.

In this research, etching resistance of two types of e-beam resists and two types of photoresists is treated by sequential infiltration synthesis (SIS). Resist patterns are sequentially exposed to trimethyl aluminum (TMA) precursor and water vapor which form alumina in the bulk, providing a high resistance under several plasma etching processes. A specially designed sample architecture is used to characterize the etching properties. During the infiltration process, the top surface of resist is cover with germanium to prevent diffusion, which presents alumina density variation on vertical direction. By observing the cross section profile after etching, the infiltration property can be analyzed.

The resistance of S1811, ma-N 1410, PMMA are greatly enhanced, that of ZEP520 is also slightly improved. A hypothesis about the principle of SIS is proposed that the bond may become saturated within the first cycle of SIS, which blocks the following diffusion of gaseous precursors.

Key words: plasma etch resistance, sequential infiltration synthesis, atomic layer deposition

Contents

List of Figures

List of Tables

List of Abbreviations

ALD……Atomic layer deposition
CVD.....Chemical vapor deposition
CCP……Capacitive coupled plasma
c-C_4F_8…… Octofluorocyclobutance
DRAM……Dynamic Random Access Memory
DOF……Depth-of-focus
FIB……Focus ion beam
GDP……Glow discharge plasma
ICP…… Inductively coupled plasma
KOH..... potassium hydroxide
MEMS…… Micro-electro-mechanical system
MOSFET.....Metal–oxide–semiconductor field-effect transistor
PS-*b*-PMMA……Polystyrene-block-poly (methyl methacrylate)
RIE……Reactive ion etch
SIS…… Sequential infiltration synthesis
SF_6.....Sulphur hexafluoride
TMAH.....Tetramethylammonium hydroxide
TMA……Trimethyl aluminum

Acknowledgement

I would like to first express my sincere gratitude to my thesis advisor, Dr. Ming Lu for his generous support, patience, immense knowledge and mentoring through my research and master thesis. I have enjoyed learning from him about plasma etching, vacuum and lithography technologies.

Besides my advisor, I would like to thank the rest of my thesis committee: Prof.Yizhi Meng, Prof.T. A. Venkatesh for their suggestion on my thesis.

This research was conducted at Center for Functional Nanomaterials in Brookhaven National Laboratory supported by the U.S Department of Energy. I would like to thank whole electronic nanomaterials group for providing cleanroom facilities and atomic layer deposition system, especially Dr. Charles Black for his training on March etcher, Dr. Fernando Camino for his help on Energy-dispersive X-ray spectroscopy and Dr. Mingzhao Liu and Dr. Chang-Yong Nam for their guidance on atomic layer deposition system.

I am also thankful to my classmates Feng He, Xiaoyu Wang, Xuyi Wang and labmates Pengfei Wang, Luozhou Li, Ke Du, Chieh-Jen Ku, Wen-Chiang Hong, Weiwei Song, Jun Tan, Di Wang for their advice on my research and career.

Last but not least, I take this opportunity to express deepest gratitude to my beloved parents and grandparents for their continuous support throughout my life.

Chapter I Introduction

1. Inductively coupled plasma reactive ion etching

Etching is an important processing step in the fabrication of integrated circuits to remove layers selectively and form patterned microstructures. Each wafer may undergo many etching steps before it is complete.

There are two main categories of etching – wet etching and dry etching. During wet etching, substrates are immersed in a reactive solution called etchant, the layer to be etched is removed by chemical reaction or by dissolution. During the dry etching, the layer to be etched is removed by chemical reaction and/or by physical bombardment which forms volatile products. Due to some disadvantages of wet etching, such as inadequacy for defining feature size below 1 μm, isotropy while etching (except for etching crystalline materials), potential of chemical handling hazards, dry etching is more commonly used in modern semiconductor industry. However wet etching still has some applications in removing some non-critical layers and stripping plasma etching residues.[1]

1.1. Overview of plasma

Plasma is one of the four states of matter. It is generated from gas by ionizing gas molecules or atoms, resulting in a combination of electrons, ions and radicals. Despite the positive and negative particles, plasma remains neutral because the amount of positive charge is always identical to that of negative charge. Ionization can be induced by means of heating or strong electromagnetic field.

Three types of electromagnetic field methods are mostly used in reactive ion etching – glow discharge plasma (GDP), capacitive coupled plasma (CCP) and inductively coupled plasma (ICP).[2]

In GDP, plasma is generated by applying a high voltage between two conducting plates – the anode and cathode. Once the voltage exceeds a certain value, the gas starts to glow and conduct electricity, which means the gas has turned into plasma state. The disadvantage of this method is the requirement of a high voltage to initiate and sustain

the plasma, which results in a high ion energy reaching the cathode. In this case, physical bombardment is favored over chemical reaction, lowering the chemical selectivity. So GDP method is more often used to sputter materials.

In CCP, the plasma is generated by a radio-frequency (RF) power supply which is typically at 13.56 MHz. In the time-varying electromagnetic field, electrons oscillate and collide with the atoms/molecule to produce further ionization. The anode plate and RF power supply are isolated by placing a capacitor between them, then anode plate attracts positive charges to accumulate on it, resulting in a potential difference between the plasma and the plate. The potential will drive positive ions towards the negative plate to perform plasma etching.

In ICP, the plasma is also generated from a RF power supply as CCP, but the difference is that the RF is delivered inductively with a coil around the RIE plasma discharge region. The time-varying RF source results in a changing magnetic field. Meanwhile the magnetic field induces an electric field, from Maxwell's theory, which circulates the plasma in the plane parallel to the lower electrode plates.

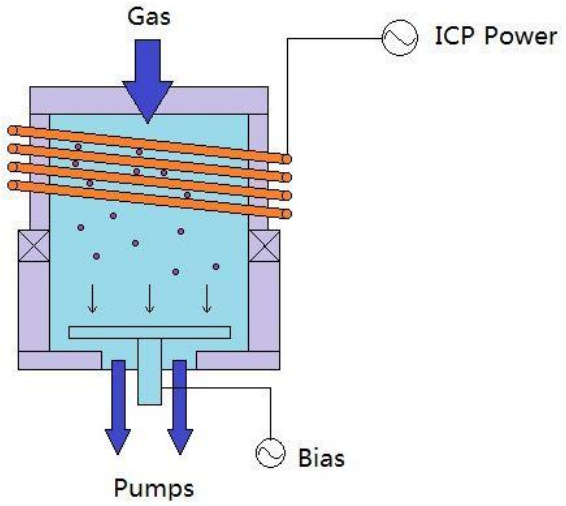

Figure 1.1 Schematic diagram of ICP reactive ion etch

1.2. Principle of reactive ion etch

In RIE, the ions are accelerated towards the sample directionally, which performs an anisotropic etching.

RIE is consisted of two noticeable effects simultaneously – physical bombardment and chemical reaction. In the physical bombardment, the layer to be etched is stripped away by the impact of the ions. In this process, selectivity is very poor, because the attack of high-energy ions has no preference between mask and substrate material, but the anisotropy is pretty high. In the chemical reaction, reactive gas is excited to create

reactive species (free radicals and reactive atoms) which can react with substrate material. The gases (typically containing chlorine or fluorine) are carefully selected to minimize the reaction with photoresist to obtain a high selectivity.

There is also a combination of physical attack and chemical reaction where directional ion bombardment can improve the chemical reaction. By adjusting the gas composition, pressure and plasma conditions, a profile with good critical – dimension control and selectivity can be achieved.

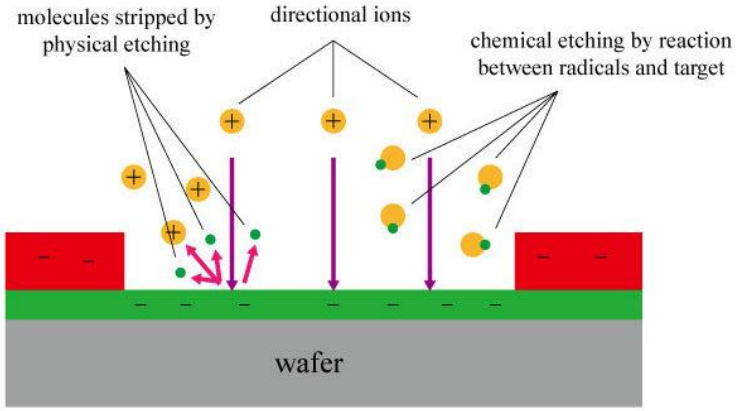

Figure 1.2 Schematic diagram of reactive ion etch

Nowadays, RIE is typically performed with a high density plasma source to define critical layer. Because for geometries under 0.25 μm, it is difficult for reactive ions to get into and the by-product to get out of the high aspect-ratio features, which will result in the slowing down or even stopping of etching at the bottom of the trenches.[3] To solve this problem, the chamber is usually operated at a much lower pressure to increase the mean free path length of the ions. But this solution gives rise to a drawback – the low etch rate due to the low density of plasma. In this case, a high-density plasma (usually an ICP source) is used to overcome the disadvantage, which can produce a degree of ionization as much as 10% compared to 0.01%-0.1% in conventional plasma. In addition, the introduction of ICP source can also provide a separate control between the plasma generation and the plasma bombardment, which is more flexible to adjust parameters to achieve desired profiles.

1.3. Deep silicon etch

Silicon etching is the one of the most important and frequent processes in the industry. Deep silicon trenches are required in some applications, such as fabricating micro-electro-mechanical system (MEMS) whose etch depth ranges from 10 μm to 500 μm. Previous technique for deep silicon etch is wet etch by liquid-phase etchants like

potassium hydroxide (KOH) and tetramethylammonium hydroxide (TMAH) which are both hot aqueous caustics. Wet etch is generally isotropic and sensitive to crystallographic orientation, so it is being taken place by plasma etch in many fields.

To obtain a deep trench in silicon, the etching process should have a high etching rate, a high selectivity and an anisotropic profile.

Firstly, a high etching rate means a high throughput in the same period of time which leads to a high yield in industry. Secondly, a high preference is needed to etch silicon as compared to the mask. Otherwise, a thick mask is required to compensate the etching, which will be easy to collapse and result in a low feature size. Finally the etching profile should be anisotropic which can transfer the pattern precisely from the mask to substrate.

Till now, two types of etching methods can achieve deep silicon etch – Bosch silicon etch and cryogenic silicon etch. Both methods include a passivation process to consolidate the sidewall and prevent it from being etched, which can improve the anisotropy.

1.3.1. Bosch etch

Bosch process is a patented process developed by Robert Bosch GmbH. It is a type of pulsed mode which contains two alternate steps to achieve a vertical profile. Bosch etch must be conducted in a high – density plasma system, such as ICP. It uses a fluorine based gas (usually sulphur hexafluoride (SF_6)) to etch the silicon and a fluorocarbon gas (usually octofluorocyclobutance(c-C_4F_8)) to offer sidewall passivation and mask protection.

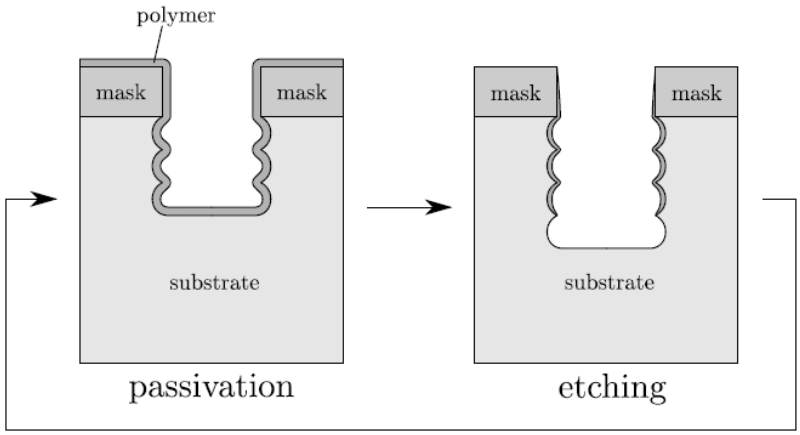

Figure 1.3 Schematic diagram of Bosch etch (Cited from http://www.iue.tuwien.ac.at/phd/ertl/node68.html)

Each breaking down and passivating step form a cycle. A complete process may consist of many cycles to obtain expected thicknesses. Within each cycle, the passivation layer which is a fluorocarbon polymer deposits on the entire substrate (including the sidewall and bottom surface) and prevents further etching. However in the following etch step, the directional ions hit the bottom surface and bombard the passivation layer on that. The silicon underneath will be exposed to the plasma, react with free radical fluorine to form volatile product.

1.3.2. Cryogenic etch

Cryogenic etch process is continuous compared to Bosch etch which is composed of several discrete cycles. It is usually performed under the temperature from -80 ℃ to -140 ℃. It uses SF_6 to provide fluorine radicals which will react with silicon to form SiF_4. SiF_4 can be removed since it is volatile. Unlike Bosch etch which uses fluorocarbon polymer to protect the sidewall, cryogenic etch uses a blocking layer of oxide/fluoride (SiO_xF_y) to provide the sidewall protection. Meanwhile the low temperature can also decrease the etching rate of the mask material as well as inhibit the etching on the sidewall by the fluorine radical. Cryogenic etch can be performed in a normal RIE system which is unlike Bosch etch. However, a high-density plasma system is highly recommended for the high density of free radicals without increasing ion density.

The cryogenic etch is temperature-sensitive. The low temperature may limit the thickness of the resist which will result in cracking if too thick, so a layer of silicon oxide may be introduced as etch mask.[4]

1.3.3. Mask selection

Mask for deep etch should be capable of transferring the fidelity of pattern to the substrate. To achieve a deep trench, a mask of high selectivity over substrate is needed. Otherwise a thick mask is required, which will cause other detrimental problems. Also a low selectivity may lead to the mask edge erosion easily, thus impart roughness and undesired structures on the sidewall under the mask. For all the reasons above, mask of high selectivity is highly required for deep etch. Oxide, metal and resist are conventional etch mask.

Silicon dioxide is the typical oxide mask and has a high selectivity. Silicon dioxide is required to be patterned by the resist on top after growth or deposition. The introduction of resist increases the number of process steps, which will complicate the process and introduce the difficulty of transferring the pattern accurately from top layer to bottom layer.

Metal mask, such as chrome, can also provide a high selectivity due to its low chemical activity in fluoride chemical. However since metal is conductor, image force (the electrostatic force on a charge in the neighborhood of a conductor, which may be thought of the attraction to the charge's electric image) may occur during the etching process, which will cause notching beneath the surface of metal mask. In addition, the scraps bombarded by ions may redeposit on the substrate and mask the material to be etched, causing undesired structures. Particularly, in cryogenic etch, the oxygen radicals will deactivate around the edge of chrome mask, thus weaken the passivation.[2]

Since it is typically impossible to pattern oxide and metal directly by lithography, the pattern has to be transferred from an upper layer of resist. That means an exposure step on resist is inevitable regardless of the mask material on substrate to be etched. Photoresist and e-beam resist are two conventional resists which are sensitive to particular wavelength light and electron beam respectively.

Compared to oxide and metal, resist mask always offers the simplest way of patterning. It provides a better sidewall protection than oxide, which results from the etched resist.[2] However, in some cases, the resistance is not sufficient to withstand the process time to obtain expected depth. In order to achieve deep etch, one can simply use a thick resist layer. However, this will result in several other problems.

In photolithography, to obtain a high resolution pattern, a well-focused image is highly required throughout the thickness of photoresist. However, due to the decrease of depth-of-focus (DOF) as a drawback of the improvement of resolution along with the development of photolithography technology, a thick photoresist may not be fully exposed since it exceeds the DOF and a focused image is not guaranteed. Other than that, the thickness of the photoresist is also limited by the collapse in the following development and baking process. The surface tension of the developer will drag and distort the high aspect-ratio pattern.[56]

In e-beam lithography, the electron forward which determines the spatial resolution will become more serious along with thicker resist, since the primary electrons have more chance to scatter laterally from the beam-defined spot. That results in a broader beam and a low resolution at the bottom of the resist. Decreasing the thickness of the resist is one way to minimize the forward scattering effect.[7-9]

Recently several new mask materials and techniques are introduced. Aluminum oxide (alumina) can offer a fairly high selectivity of 5000:1, so just a thin layer is required for patterning. The alumina mask is always patterned by lift-off instead of conventional methods. Aluminum oxide is insulator, the image force induced by metal mask can also avoided. Another new technique for masking is gallium implantation by focus ion beam (FIB). [10] [11] The gallium-implanted area has different etching

characteristics with unimplanted area. The gallium implantation will render the silicon substrate high resistant to chemical etching. This method can directly pattern the substrate into any shape as well as circumvent the use of resist, which will save process time and steps. It can be utilized in developing the prototype of electrical devices. However, since the pattern is written gradually by ion beam, the drawback is the low throughput. Also the removal of the gallium-implanted mask is still a problem.

2. Atomic layer deposition

2.1. Introduction of ALD

Atomic layer deposition (ALD) is a newly emerged technique which is able to deposit thin films on different substrates with atomic scale precision. ALD can be utilized in semiconductor industry to fabricate high dielectric constant gate oxides in the MOSFET and copper diffusion barriers in backend interconnects. In addition, it has also met the requirement for depositing high quality dielectrics in the trench capacitors for DRAM.

After the invention of ALD,[12] no substantive breakthrough was made until 1990s due to the complexity of surface chemical reaction and low deposition rate. Recent years, miniaturization in the semiconductor industry has impelled the advancement of ALD technique to grow pinhole – free, conformal thin films with atomic level control, which no other techniques can achieve. Because of the requirement of smaller dimensions and thinner layer, low deposition rate is no longer a problem.[13]

ALD is a variant to chemical vapor deposition (CVD), but its mechanism is totally different. In CVD process, volatile precursors are mixed in a chamber to react or decompose on the substrate continuously, while in ALD process, precursors are kept separately throughout the whole process and introduced into the chamber by short pulses sequentially. Only monolayer can be deposited within each cycle.

The mechanism of ALD operates as follows:

(a) Expose the first precursor which is usually organometallics

(b) Purge the chamber to remove the extra or unreacted gaseous precursor

(c) Expose the second precursor or activate the surface

(d) Purge the chamber again

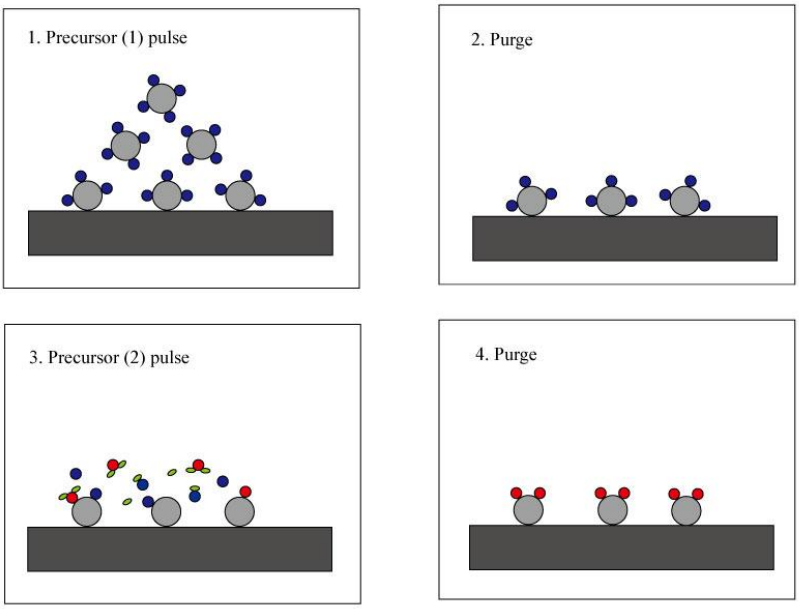

Figure 1.4 Flow chart of atomic layer deposition

The above four steps constitute a cycle and can repeat sequentially to deposit film of expected thickness. The process is self-limiting so that the layer can be extremely smooth and conformal to the substrate. Other than that, since the process is controlled at monolayer which means angstrom level, the thickness can be fairly precise.

2.2. Semi-dynamic mode of ALD

Thin film deposition in an ALD system is always dynamic and continuous, with frequent switch between metal precursor and water or ozone precursor. However in high aspect-ratio structures, the continuous flow and the cross flow do not allow gaseous precursors to diffuse deeply into the trench, the film will grow only on the shallow sidewall as shown in Figure 1.5, which cannot cover the entire structure.

Therefore a semi-dynamic mode of ALD is introduced for coating high aspect-ratio (>1:15) structures or coating particles and porous materials.

While in the semi-dynamic mode,

(A) the chamber is isolated from ambient before the pulse of precursor;

(B) sufficient time is rendered for the diffusion of precursor into the entire trench;

(C) purge the excess gaseous precursor or byproduct;

Then repeat for the second precursor.

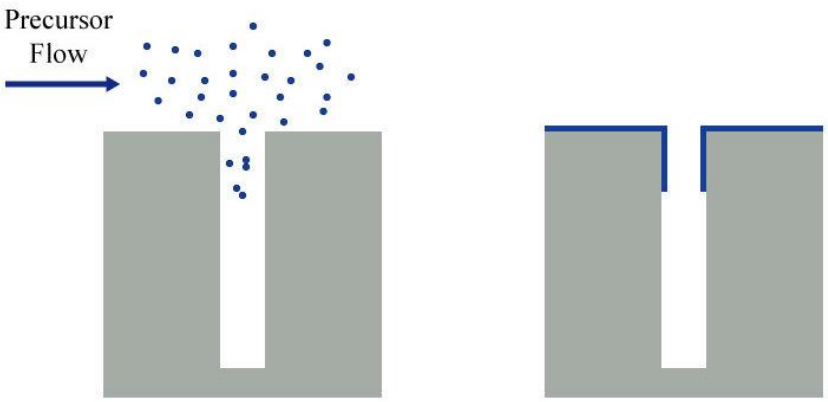

Figure 1.5 Schematic diagram of dynamic mode on high aspect-ratio structure

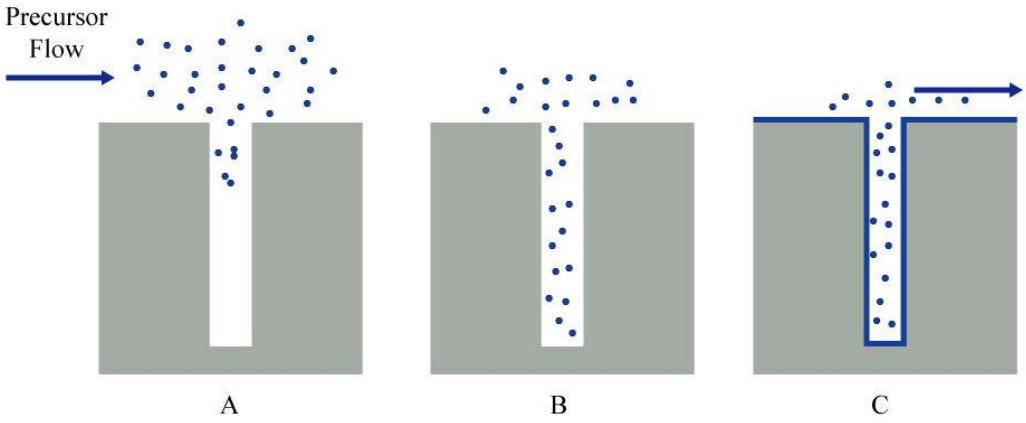

Figure 1.6 Schematic diagram of exposure mode on high aspect-ratio structure

3. Sequential infiltration synthesis by ALD

As stated above, resist mask is the easiest method for masking compared to the other masks like metal and oxide which need to pattern resist first or gallium implanted silicon which has a low throughput. If etching resistance of resist can be improved, the pattern transfer process will be simpler and more direct.

There are several schemes previously reported to enhance the etch resistance. Some of these methods are based on the infusion of silicon into resist films called silylation, which however only modify the surface of the resist without providing any protection on sidewalls.[14-17]Another method is a top surface imaging method which uses area selective ALD on chemically amplified polymer resist films. In this scheme, resist film is selectively exposed to create reactive hydroxyl sites on the film surface.

And the exposed sites can subsequently act as nucleation sites in the deposition of metal oxide by ALD. The metal oxide layer can be used as etch barrier layer in the resist plasma etch by oxygen, which transfers pattern from barrier layer to resist. However this method also lacks the bulk protection.[18]

Recently an approach using sequential infiltration synthesis (SIS) in self-assembled block copolymer lithography has emerged,[19-21] which can render a fully bulk enhancement. Self-assembled thin films can make periodic nanostructures in large scales at low-cost, which is promising in for microelectronics and date storage.[22-29] SIS process is always performed in an atomic layer deposition chamber with semi-dynamic mode. In this process self-assembled block copolymer, polystyrene-block-poly (methyl methacrylate) (PS-*b*-PMMA) is exposed to metal and H_2O precursors alternatively. Due to the long exposure time in semi-dynamic mode, precursors infiltrate into resist, the selective reaction of trymethyl aluminum with PMMA phase provides a site for Al_2O_3 growth. After the removal of PS phase by oxygen plasma, the remaining PMMA phase would survive since the interior alumina is resistant to the oxygen plasma. Then the patterned PMMA can be used directly as etch mask without other intermediate layer. The size and shape of ordered domains can be adjusted by changing weight and chemical composition, which will provide different patterns.[30-32]

However, since feature size of PS-*b*-PMMA is always in the range of dozens of nanometers, it seems that the PMMA phase is fully filled with alumina, the modified characteristic of etching resistance of PMMA has not been fully studied, thus limit the application of this method

4. Purpose of this research

SIS is an emerging technique which can be used in the industry in the next few years to modify the etching resistance of resist, then avoid the use of thick resist layers or intermediate layers, thus provide an easy and low cost method to achieve high-resolution features.

In this research, two types of e-beam resist (PMMA950 and ZEP520) are deeply investigated, meanwhile, two types of ultraviolet photoresist (S1811 and ma-N 1410) which are widely used in microelectronics and microsystems technology are also investigated. In chapter II, the preparation of the sample which is used to study etching resistance will be described. In chapter III and chapter IV, I will analyze the infiltration depth of precursors and SIS enhancement mainly from the SEM images, then propose possible mechanism of the SIS process.

Chapter II SIS sample preparation for etching performance test

1. Process design

Generally the infiltration happens from all directions which is shown in Figure 2.1, but it is difficult to study the modified resistance and infiltration depth in this case. A specially designed thin film stack system is used to isolate the one-dimensional properties from this conformal thin film process. We employ a thin germanium layer to block the diffusion on the top surface, allowing diffusion of precursors only from sidewalls as shown in Figure 2.2. Within the SIS step, TMA is infiltrated into the bulk of resist in form of gas precursors and forms alumina in the resist matrix. The density of alumina will drop along the normal direction into the resist. After the removal of germanium layer, the hardened resist is subjected to three typical etch recipes.

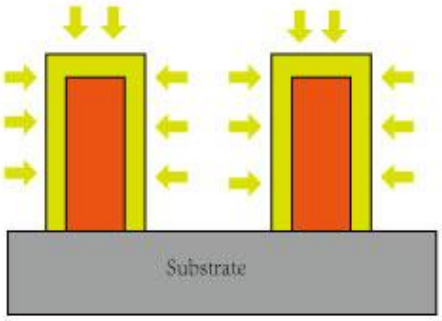

Figure 2.1 SIS from all directions

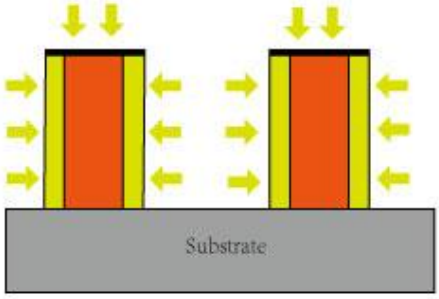

Figure 2.2 SIS only from sidewalls

Depending on the difference of alumina density on horizontal direction, the etching rate of the resist varies and the remaining resist after etching may vary in height. Figure 2.3 lists several possible profiles after etching. By measuring the cross section profile of the resist, the modification of different resists by SIS can be revealed.

Figure 2.3 Possible etching profiles

2. Process description

1) Resist Coating: Four different resists are coated on silicon wafers respectively at different speeds and followed by different baking temperatures to get different thichnesses.

	Spin		Baking	
	Speed (RPM)	Time (s)	Temperature (℃)	Time (s)
PMMA950 A8	3K	45	110	240
ZEP520	2K	45	180	180
S1811	3K	45	110	120
maN-1410	3K	45	100	120

Table 1 Parameters for resist spin coating

Particularly, since ma-N 1410 is negative resist whose etching property is performed after exposure, it is subjected to photolithography after baking with Karl Suss MA6 Mask Aligner at xeon lamp power of 470 W, flood exposure mode for 7.5 seconds.

2) Germanium Deposition: A germanium layer with a thickness of 15 nm is deposited on the surface of PMMA950 A8, ZEP520, ma-N 1410, which can prevent Al_2O_3 infiltration from the top. The germanium layer on S1811 is 58.2nm, because thinner layer cracks due to the difference in coefficient of thermal expansion (CTE) between germanium and S1811. This step is carried out in Kurt J. Lesker PVD75 Sputtering System at an argon pressure of 3.7 mTorr after pumping down to 5×10^{-6} Torr. The deposition rate is about 1.2 Å/s at DC bias 200 W.

3) PMMA950 A4 deposition: A layer of PMMA950 A4 is coated at 5K RPM for 45 s on the surface of germanium layer followed by baking at 90 ℃ for 180 s for later

e-beam lithography patterning.

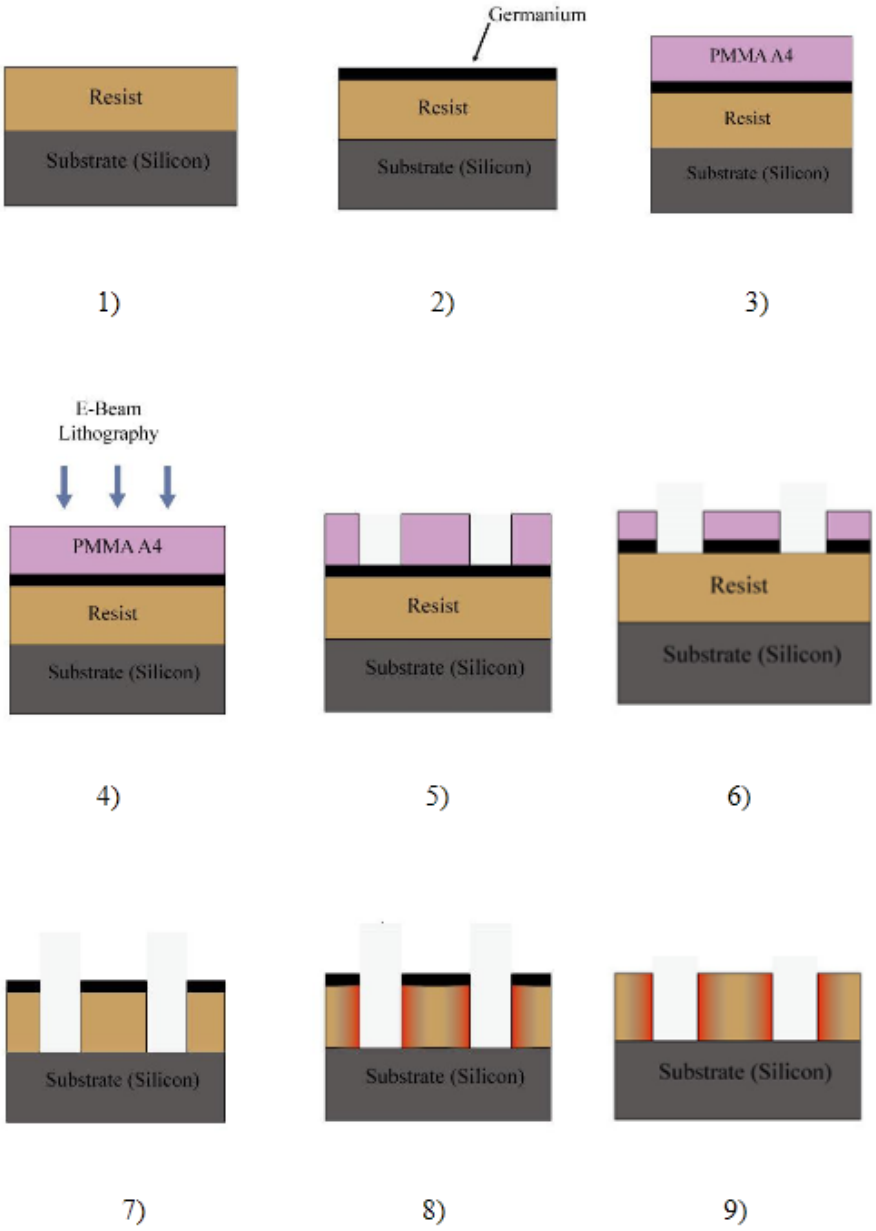

Figure 2.4 Scheme for sample preparation process

4) PMMA950 A4 Patterning: PMMA950 A4 is exposed by electron-beam lithography which presents feature sizes with four different widths ranging from about 400 nm to 1 μm.

5) Developing and Descuming: PMMA950 A4 is developed in MIBK and IPA with a mixture ratio of 1:3 for 45 s followed by rinse in IPA for 45 s. After development, a descuming step is conducted in oxygen pressure of 100 mTorr, and a power of 100 W for 3 s to strip the residual PMMA on germanium layer which may cause

undesired patterning.

6) Germanium Etching: Patterns on PMMA950 A4 are transferred to germanium layer by plasma etching using with CF_3Br in a March Etcher at CF_3Br pressure of 120 mTorr, and a RF power of 60 W, this process is carried out for 30 s for ZEP520, S1811, ma-N 1410 samples and 80 s for PMMA950 A8 samples respectively.

7) Bottom Layer Resist Etching: Patterns on germanium layer are transferred to the resist underneath by oxygen plasma etching. The RF power and gas pressure are 200 W and 30 mTorr respectively. Due to the difference in thickness and etching rate of four resists, the process times adjusted correspondingly. The real etch times are 1.5 times of those calculated from the average etch rates and film thicknesses in advance, so that the resists are completely removed.

	PMMA950 A8	ZEP520	S1811	ma-N1410
Etch rate (nm/s)	11.5	5.2	4.5	4.8
Film thickness (nm)	880	473	1258	1004
Expected time (s)	77	91	280	210
Real time (s)	12	130	390	290

Table 2 Resist etch rates and time

8) SIS in an ALD chamber: The SIS process is conducted in a Cambridge Savannah ALD System which employs a stopvalve to achieve the isolation mentioned above. The process starts with N_2 100 sccm followed by a pumping down to clean the chamber. Then the stopvalve closes to isolate the chamber from the ambient. After that TMA is pulsed into the chamber for 0.014 s followed by a waiting time of 300s for the precursor to fully diffuse into the bulk of resist. Then the stopvalve opens allowing the N_2 flow to remove the rest of TMA. The stopvalve closes again followed by a H_2O pulse of 0.045 s and a waiting time of 300 s for TMA to react with H_2O to form alumina. At last a N_2 flow is also needed to remove the byproduct and remaining H_2O.

   Since the glass transition temperature (T_g) of PMMA is 90 ℃, the ALD process is performed at 85 ℃ to stay away from resist flow. The ALD process is carried out for 1 cycle, 3 cycles, 6 cycles and 9 cycles respectively to explore the influence of cycles on different types of resists.

9) Al_2O_3 Breakthrough after ALD: During the sequential infiltration process, besides

the alumina infiltration into the bulk of resist, a thin layer of alumina is also deposited on the surface of germanium and silicon substrate as well as on the sidewall of resist. Since alumina has high resistance to most etch recipes, alumina on the surface must be stripped for subsequent step. This step is performed in Oxford Plasmalab100 System at a pressure of 5 mTorr, RF power 200 W, ICP generator power 1000 W and BCl_3 20 sccm, Cl_2 5 sccm. Process duration time varies corresponding to different cycles.

10) Germanium removal: The germanium is removed by CF_3Br plasma etch at 120 mTorr, 60 W for 30 s so that the resist surface is exposed to the following plasma etching process.

Chapter III Etching resistance of SIS treated resists

1. Plasma etch of the SIS treated resist

The four resists are subjected to three typical etch recipes – oxygen polymer etch, cryogenic silicon etch and silicon oxide etch. Oxygen polymer etch is a typical chemical etch process. In cryogenic silicon etch process, since the bias voltage etch is generally between 15 V and 20 V, chemical etch is favored over physical etch, a smoother profile can be achieved compared to Bosch etch.

	Pressure (mTorr)	RF power (W)	ICP power (W)	Gas Flow Rate (sccm)	Temperature (℃)
Cryogenic Si Etch	12	15	800	SF_6=40 O_2=18	-100
O_2 Polymer Etch	30	200	0	O_2	20
SiO_2 Etch	15	40	700	CHF_3=50 O_2=1.5	20

Table 3 Plasma etch processes

Particularly, the mechanism of SiO_2 etch need to be illustrated here. Because of the presence of a thin layer of fluorocarbon on SiO_2 through etching, which dramatically influences the etching mechanism, the SiO_2 etching process comes into three distinct regimes of behavior in the SiO_2 etching process by CHF_3 – "reactive sputtering regime", "fluorocarbon suppression regime" and "fluorocarbon deposition regime" successively from low to high self-bias voltage.[33]

The fluorocarbon layer is formed due to the overwhelming polymerization ablity of a high-density discharge. At high bias voltage, the SiO_2 etching rate is subjected to a theoretical oxide reactive sputtering curve as shown in dashline in Figure 3.1. When bias goes lower, the fluorocarbon suppression regime takes over. In this regime, a steady state thin layer of fluorocarbon forms with a thickness from 0.2 nm to 1 nm. The SiO_2 etching rate is suppressed due to a complex process of ion energy dissipation within the fluorocarbon film. In addition, the thickness of fluorocarbon

film plays an important role in the etching rate, causing up to 300 – 400 nm/min variation in etching rate by only 2 monolayer film. When bias continues decreasing into fluorocarbon deposition regime, fluorocarbon film deposition dominates, which impedes the SiO_2 etching. Therefore SiO_2 is always performed at high bias voltages, at which physical bombardment is really strong and dominates the etching process over chemical etch.

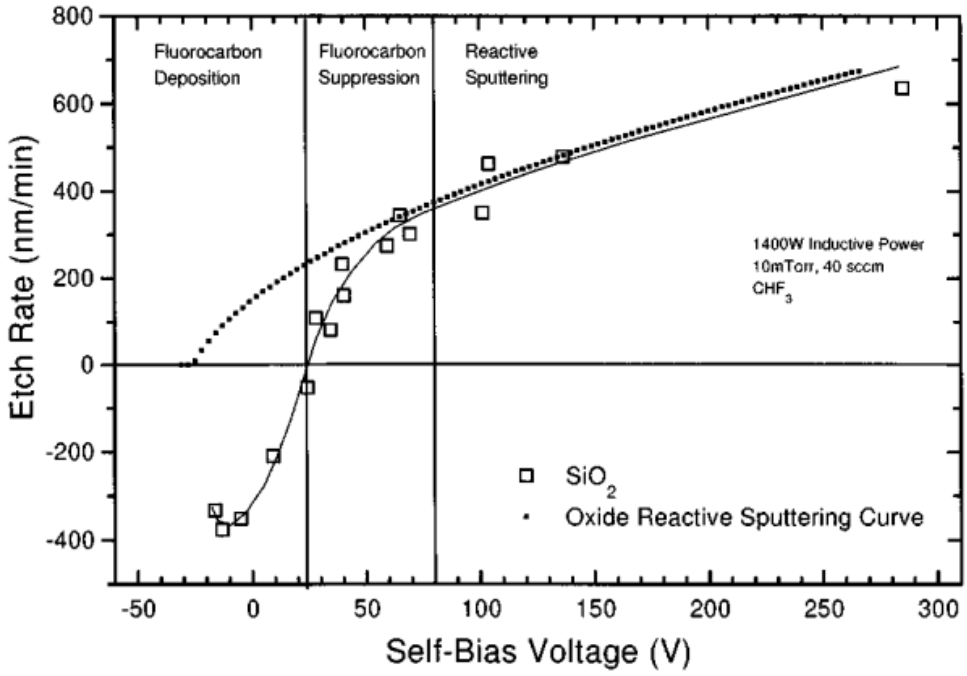

Figure 3.1 Etch rate vs dc self-bias voltage with the three silicon dioxide processing regimes outlined for 10 mTorr processing conditions (Adapted from N. R. Rueger, J. J. Beulens, M. Schaepkens, M. F. Doemling, J. M. Mirza, T. E. F. M. Standaert and G. S. Oehrlein, *J. Vac. Sci. Technol. A*. 1997, 15.1881)

2. Scanning electron microscope imaging

Cross sectional images of all the resist samples are captured by Hitachi 4800 Scanning electron microscope. Several effects may influence the picture quality. Since resist material is insulator which doesn't conducting electrons, electrons will aggregate on resist and cause a nonuniform distribution, which will result in electrostatic force to repel or drag resists, thus distort the profile of resist. Other than that, the heat from electrons probably may melt resist to some extent. Also, what is more severe in e-beam resist imaging, the resist is exposed by electrons and becomes cross-linked or flexible that has a negative effect on imaging.

For the reasons above, a thin layer of gold is highly needed to be deposited on the resist, enhancing conductivity and reducing the heat and exposure effect. The thickness of gold film should be as thin as to perform clear interface between resist and substrate, and as thick as to sufficiently improve conductivity. After trying with different gold

film thicknesses ranging from 1.85 nm to 5 nm, we find 2.5 nm seems to offer the best image quality.

The accelerating voltage also plays and important role in imaging. Even though a high accelerating voltage leads to a smaller probe diameter to decrease lens aberration and thus a better resolution, it could deform the feature due to charging effect (High voltage results in deep penetration of the electrons therefore voids the conductive layer on the surface) and obscure the surface details which is fairly important here. Here we choose 1 keV instead of 5 keV to obtain a better image.

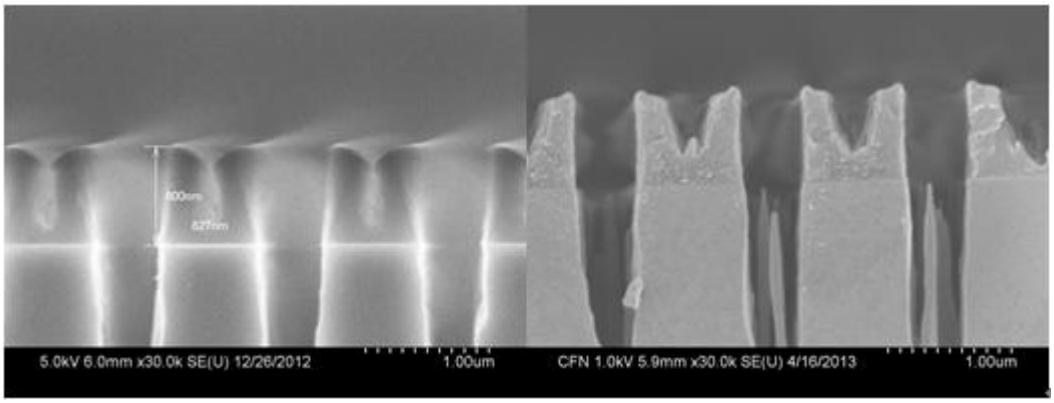

Figure 3.2 Comparison between PMMA images captured under high accelerating voltage without gold film (left) and PMMA images captured under low accelerating voltage with gild film (right)

3. PMMA950 etching resistance analysis

3.1. Introduction to PMMA

Poly (methyl methacrylate) (PMMA) is a transparent thermoplastic, often used as a lightweight or shatter-resistant alternative to glass. Chemically, it is the synthetic polymer of methyl methacrylate as shown in Figure 3.3. In semiconductor research and industry, PMMA is used as a resist in electron beam lithography process since it is sensitive to electrons. Exposure to electron beam will create chain scission, allowing for the selective removal of exposed areas by chemical developer. PMMA products are formulated with 495K or 950K molecular weight, and denoted as PMMA495 and PMMA950 respectively. In this research, PMMA refers to PMMA950.

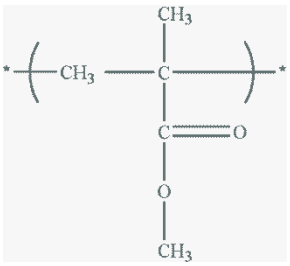

Figure 3.3 Chemical structure of PMMA

3.2. PMMA etch profile after 45 seconds oxygen etch

Firstly, I need to define two parameters that will be frequently mentioned in this chapter – the survived height and effective depth. The survived height refers to the difference of height between the outermost part which is fully enhanced and the centermost part which is not enhanced at all. The effective depth refers to the distance from the outermost edge horizontally to the interface where there is no etch resistance, which is observed in the SEM images.

Figure 3.4 shows that PMMA with a linewidth of about 400 nm is fully resistant to oxygen etch, which indicates that Al_2O_3 has completely diffused to the center of the feature from both sides of the sidewall. Also the number of cycles doesn't matter at all here, 1 cycle of ALD SIS can provide sufficient enhancement.

For 600 nm linewidth (Figure 3.5), PMMA starts to be incapable of withstanding the O_2 plasma, a trench appears in the center position of the feature, which means 200 nm is the upper limit of diffusion depth to render resistance to oxygen plasma. Also Figure 3.6 shows that although the top surface seems to be collapse, it is still connected, only the PMMA underneath has been etch away, providing no resistance.

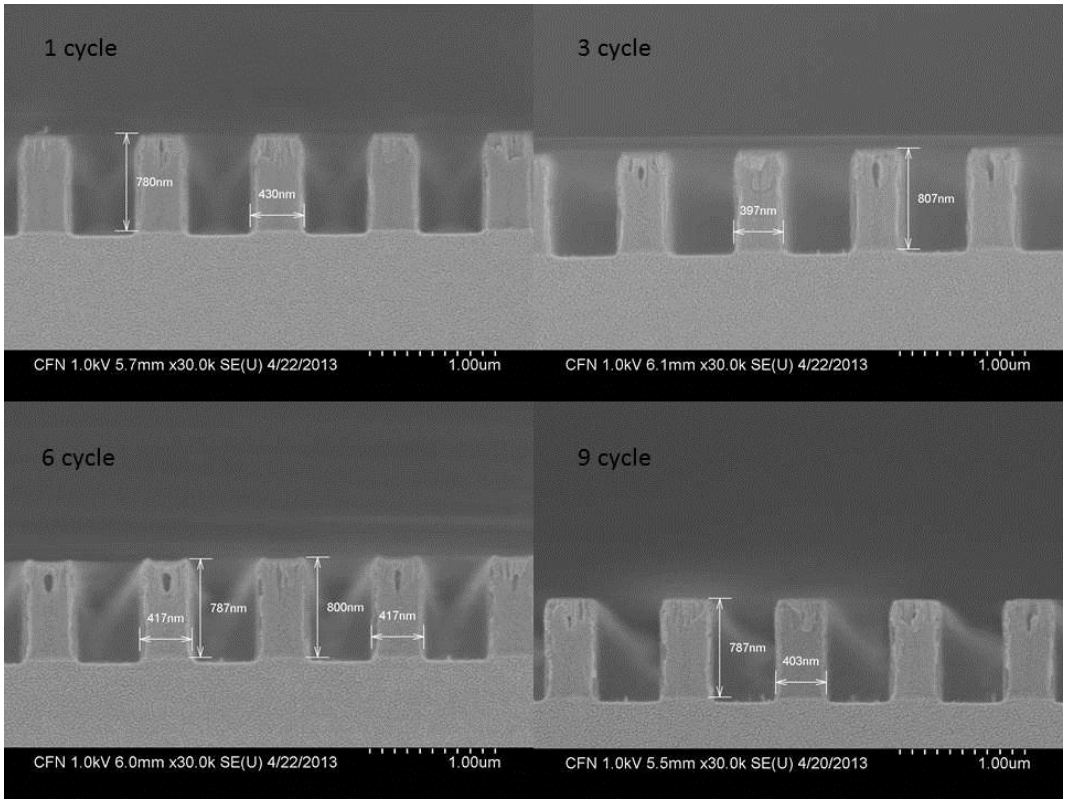

Figure 3.4 Cross section view of PMMA 1-9 cycle ALD with about 400 nm linewidth after 45 seconds O_2 etch

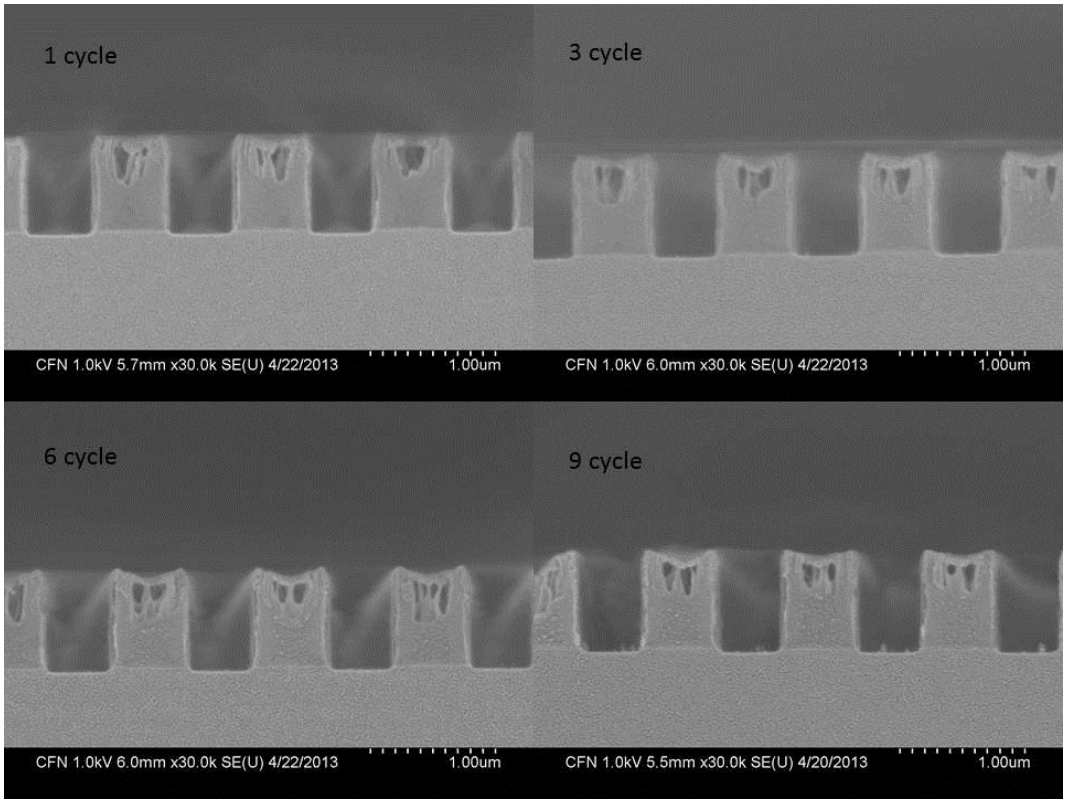

Figure 3.5 Cross section view of PMMA 1-9 cycle ALD with about 600 nm linewidth after 45 seconds O_2 etch

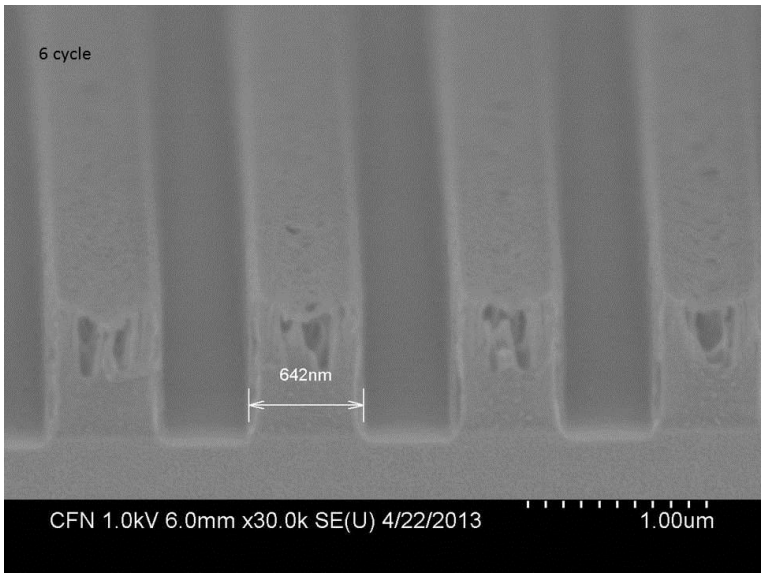

Figure 3.6 PMMA 6 cycle ALD with 600 nm linewidth after 45 seconds O_2 etch

For linewidth of 800 nm and 1 μm, the two sides of the sidewalls become completely separate. From Figure 3.7 to Figure 3.11, we can see that within the first 200 nm from the edge of sidewall, SIS renders a fairly high improvement of resistance and only a slight slope is observed. Beyond 200 nm, an apparent slope appears when it goes deeper towards the center horizontally, announcing a significant decrease in

etching resistance. This slope continues until about 350 nm from the sidewall edge.

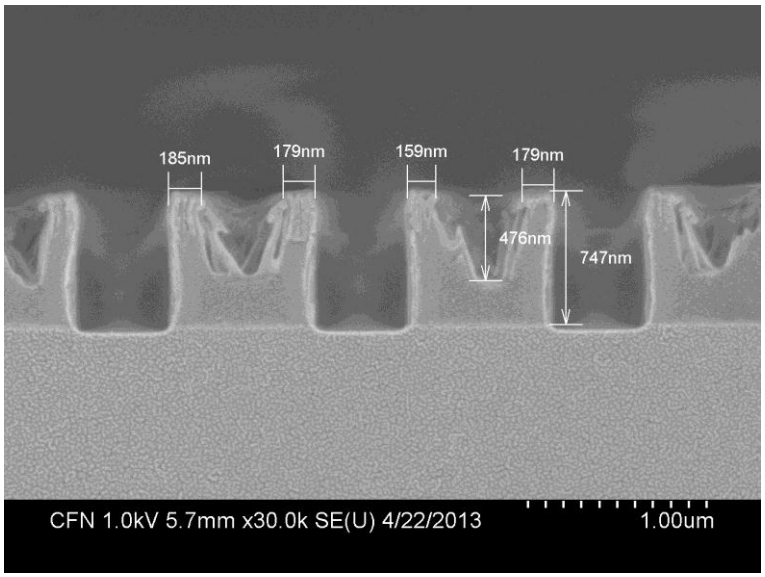

Figure 3.7 Cross section view of PMMA 1 cycle ALD with 800 nm linewidth after 45 seconds O_2 etch

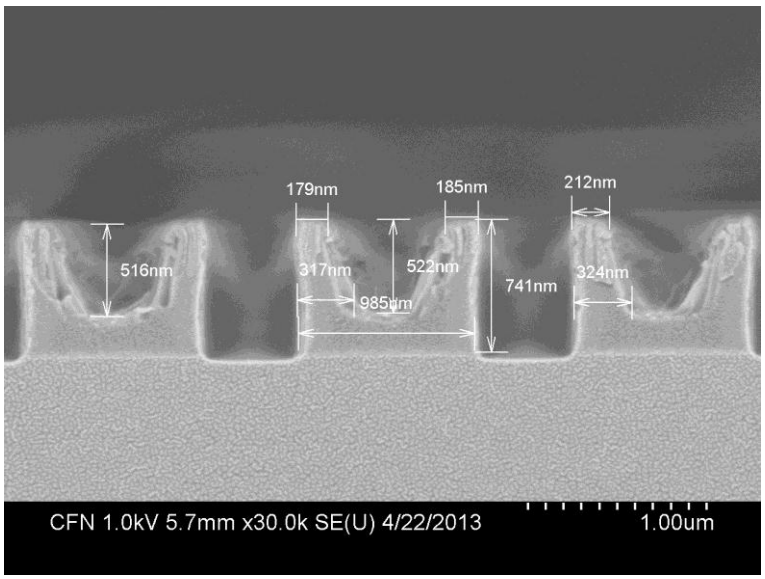

Figure 3.8 Cross section view of PMMA 1 cycle ALD with 1 µm linewidth after 45 seconds O_2 etch

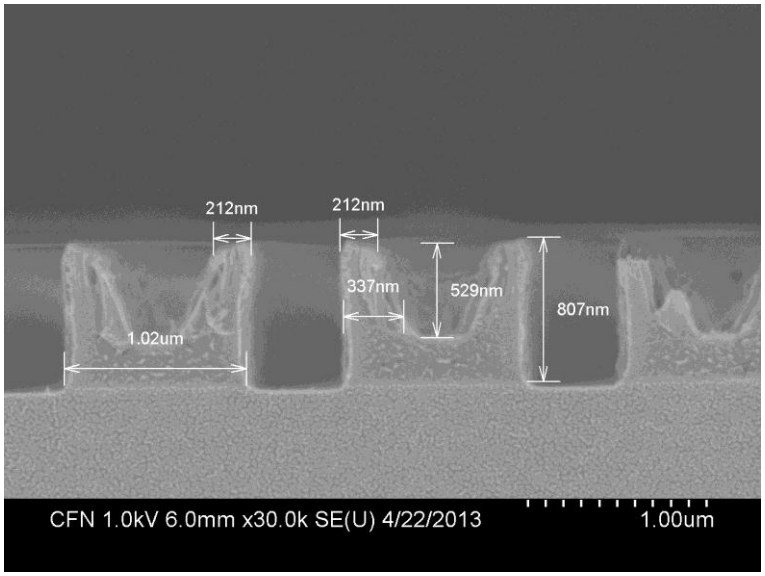

Figure 3.9 Cross section view of PMMA 3 cycle ALD with 1 µm linewidth after O_2 etch 45 seconds

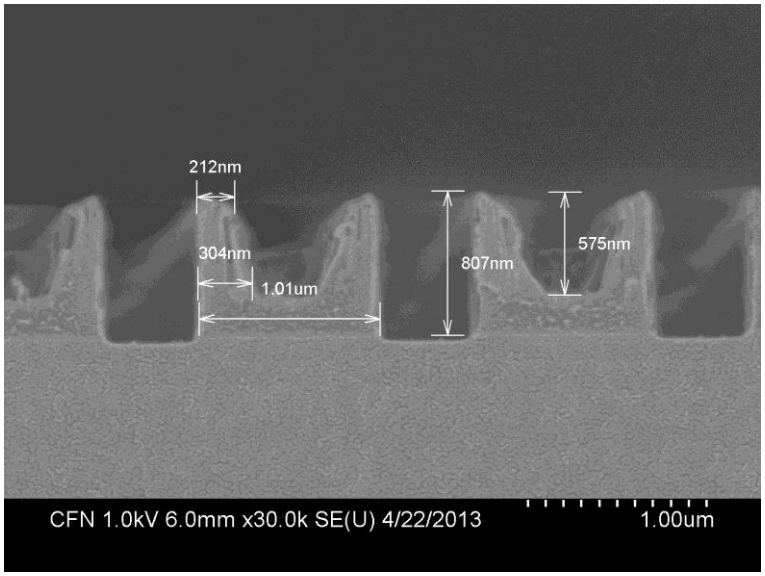

Figure 3.10 Cross section view of PMMA 6 cycle ALD with 1 µm linewidth after O_2 etch 45 seconds

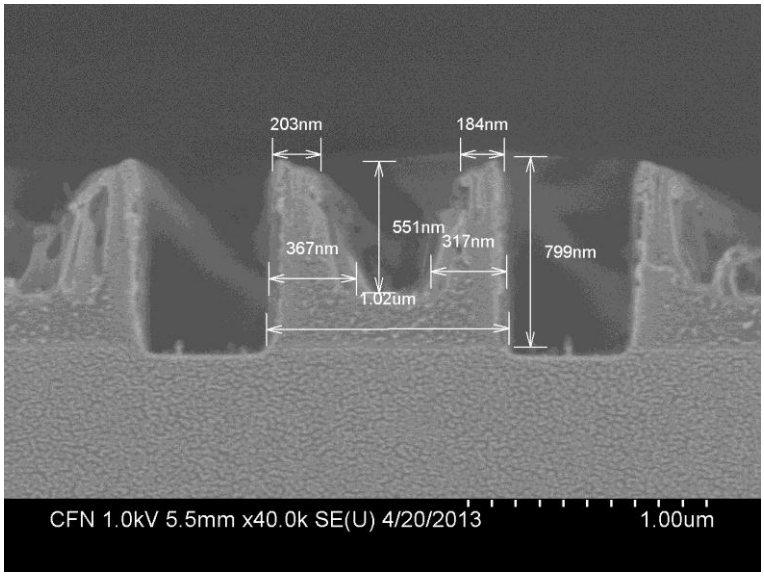

Figure 3.11 Cross section view of PMMA 9 cycle ALD with 1 μm linewidth after O_2 etch 45 seconds

In Figure 3.12, the etching rate performs a significant drop beyond a constant etching rate, which means two effectively enhanced parts has fully separated.

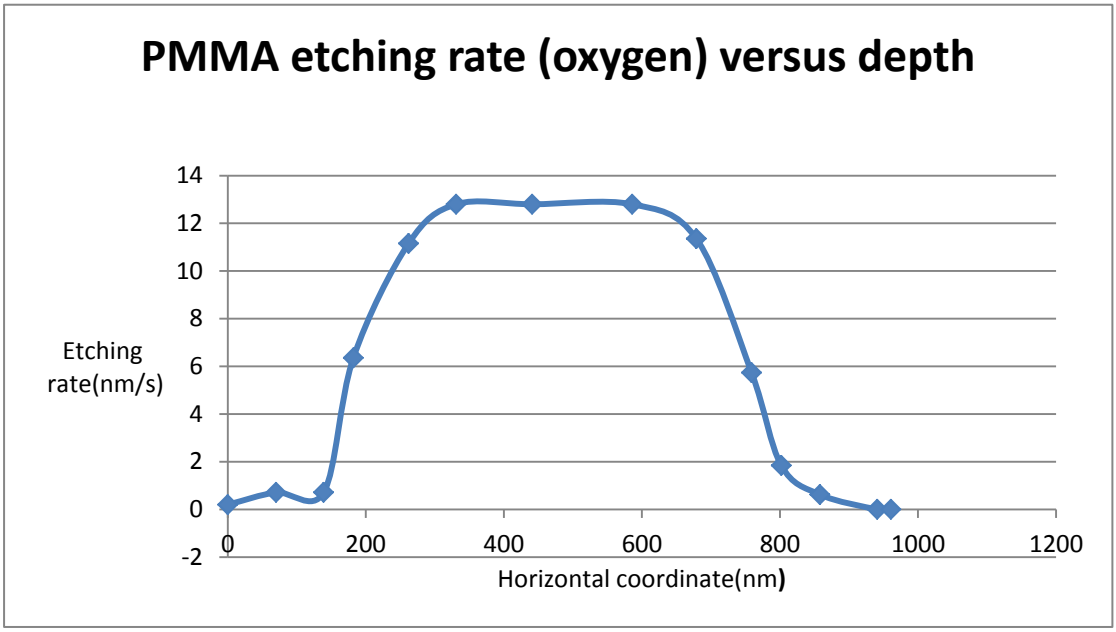

Figure 3.12 Etching rate (O_2) of 6 cycle SIS processed PMMA versus depth

3.3. PMMA etch profile after cryogenic silicon etch 120 seconds

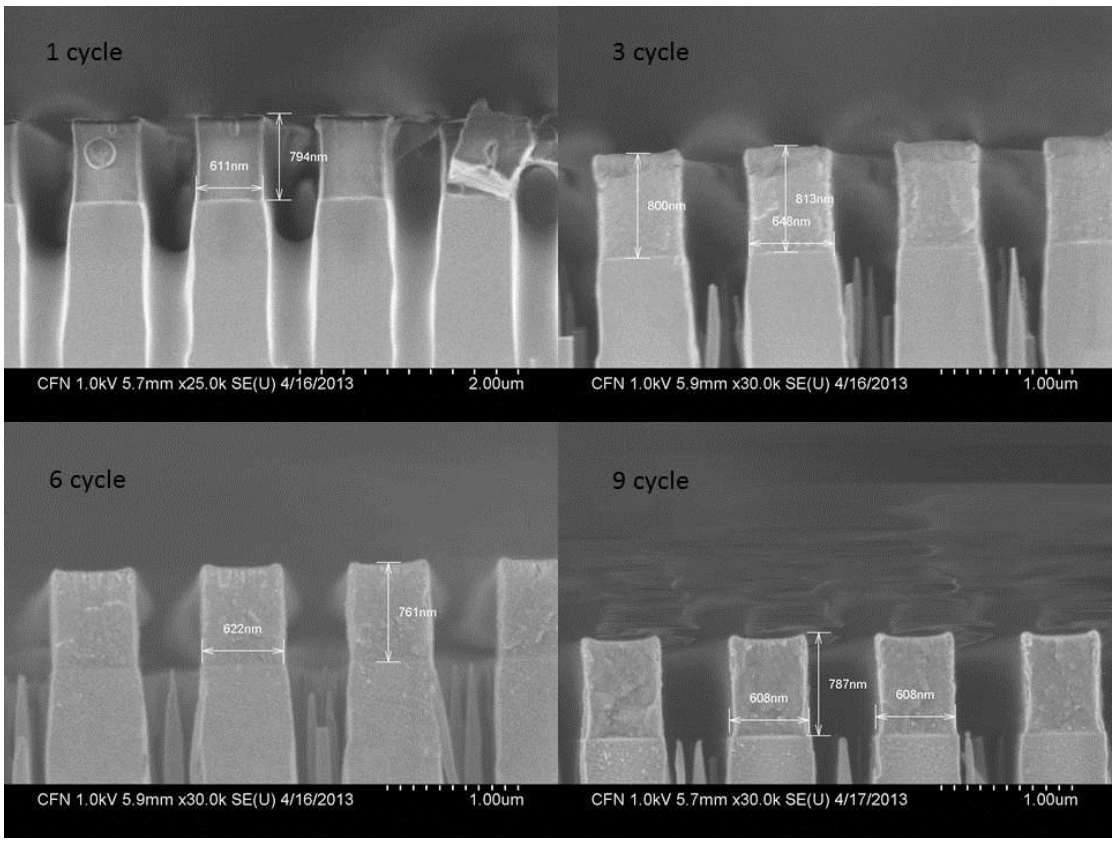

Figure 3.13 Cross section view of PMMA 1-9 cycle with 600 nm linewidth after 120 seconds cryogenic silicon etch

Figure 3.13 shows during the cryogenic silicon etch, the 600 nm feature is fully reserved instead of 400 nm in oxygen etch. (Samples are the same, just different etching processes) That is due to the higher chemical etch rate of pure O_2 plasma than SF_6/O_2 plasma on resist material which is polymer material. When the linewidth increases to 800 nm and 1 μm (Figure 3.14 – Figure 3.18), the feature starts to split as what happens to PMMA with 600 nm linewidth etched by oxygen. However the width of each splitted part on both sides is less than half of 600 nm on average. With the presence of an obvious slope, a further diffusion of the precursors with lower resistance is indicated. When the two obvious splitted parts approach in the 600 nm feature, hundreds of nanometers Al_2O_3 will superimpose, and present a high resistance to plasma. The superimposition effect also happens in the previous oxygen plasma etch.

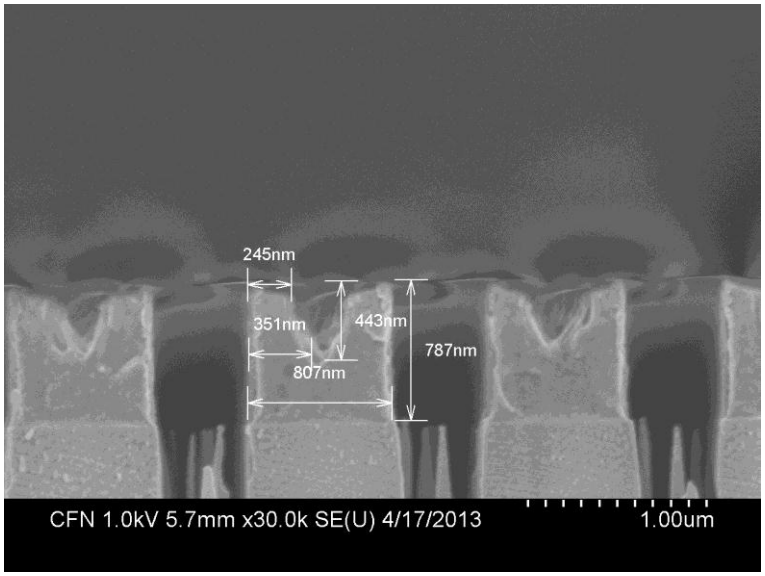

Figure 3.14 Cross section view of PMMA 9 cycle with 800 nm linewidth after 120 seconds cryogenic silicon etch

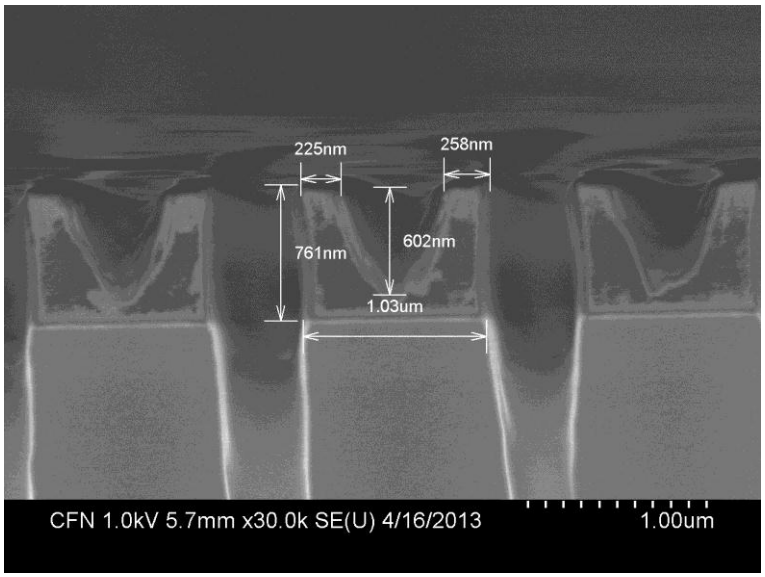

Figure 3.15 Cross section view of PMMA 1 cycle ALD with 1 µm linewidth after 120 seconds cryogenic silicon etch

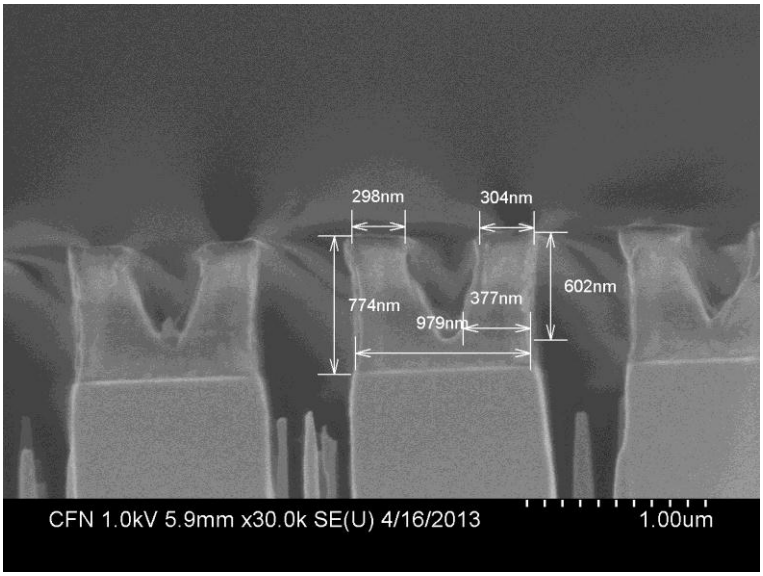

Figure 3.16 Cross section view of PMMA 3 cycle ALD with 1 µm linewidth after 120 seconds cryogenic silicon etch

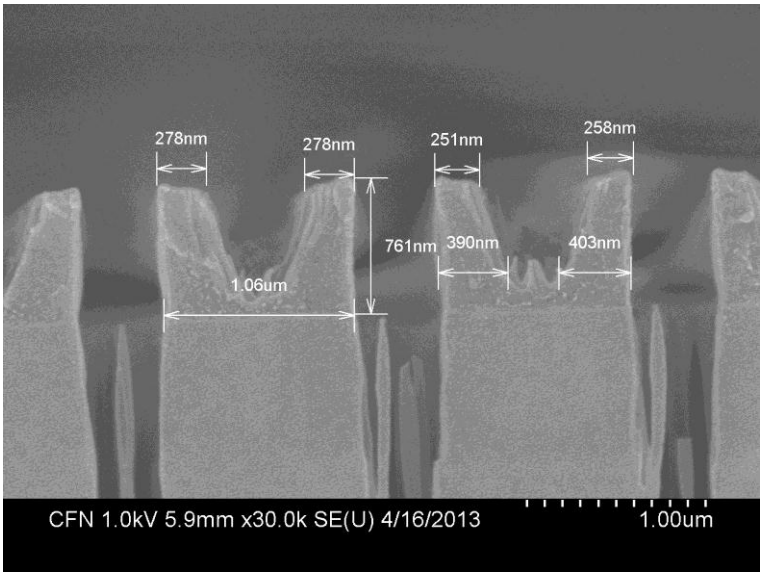

Figure 3.17 Cross section view of PMMA 6 cycle with 1 µm linewidth after 120 seconds cryogenic silicon etch

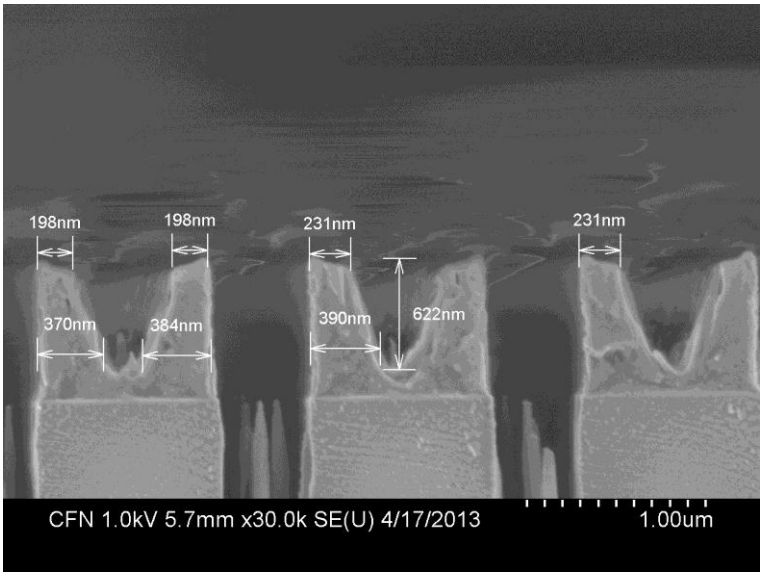

Figure 3.18 Cross section view of PMMA 9 cycle with 1 µm linewidth after 120 seconds cryogenic silicon etch

The plot in Figure 3.19 shows the silicon etching rate change of 6 cycle SIS processed PMMA on horizontal direction. When it comes from the center to the outermost edges, the etching rate performs a drop earlier than that in oxygen plasma which means a thicker effective depth.

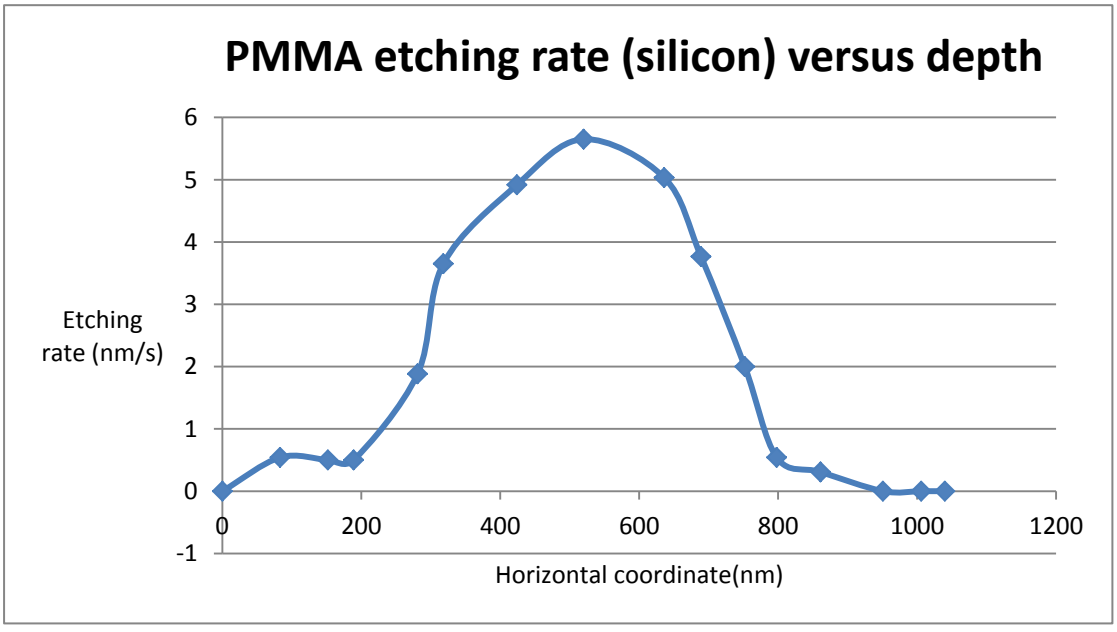

Figure 3.19 Etching rate (silicon) of 6 cycle SIS processed PMMA versus depth

Here we choose PMMA after 1 cycle ALD to analyze the etch resistance change by SIS process. The resistance against cryogenic silicon etch is improved by a factor of 6.

	Original height (nm)	Height after etching (nm)	Etch time (s)	Etch rate (nm/s)
Untreated PMMA	880	159	120	6
PMMA after SIS	880	761	120	1

Table 4 Comparison of silicon etching rate between 1cycle SIS processed PMMA and un-SIS processed PMMA

3.4. PMMA etch profile after 150 seconds SiO_2 etch

The etching profile by SiO_2 etching recipe is similar to that in oxygen etch, but with an effective depth slightly shallower than that in oxygen etch. In addition, the top of splitted features performs a steeper slope, sometimes even a pinnacle, comparing to a nearly horizontal surface in oxygen etch and cryogenic silicon etch.

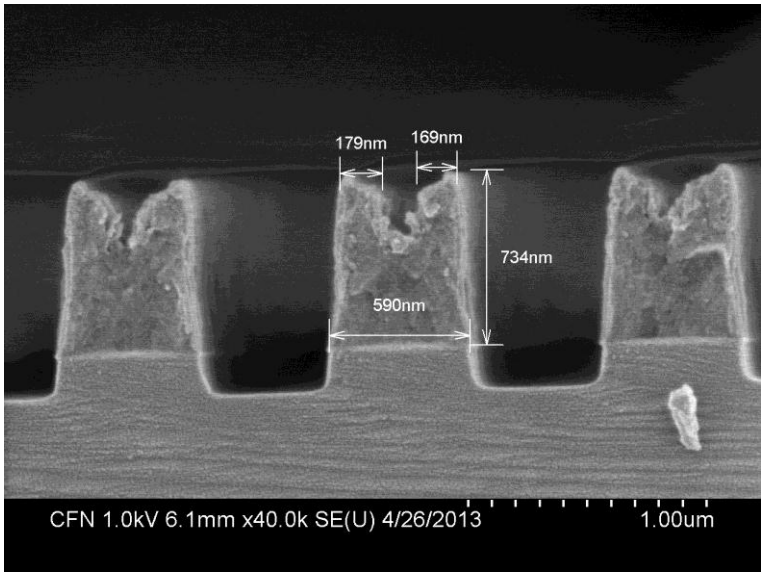

Figure 3.20 Cross section view of PMMA 1 cycle with 600 nm linewidth after 150 seconds SiO_2 etch

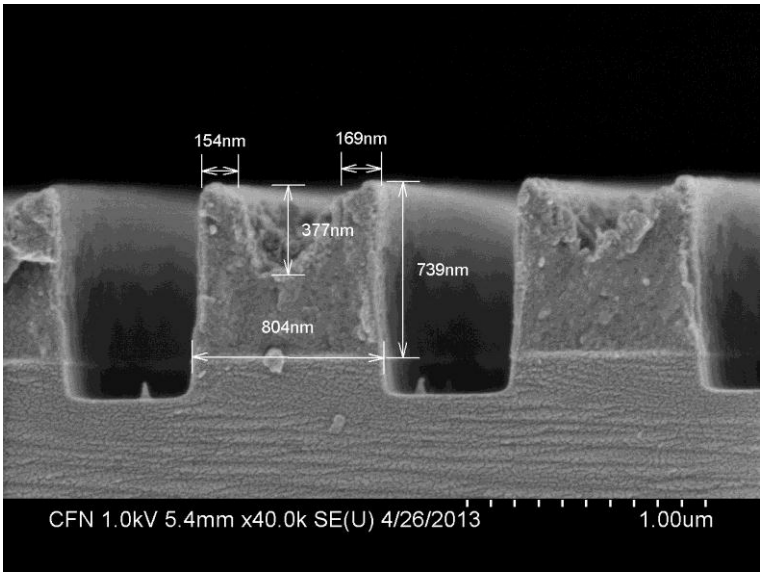

Figure 3.21 Cross section view of PMMA 3 cycle with 1 µm linewidth after 150 seconds SiO_2 etch

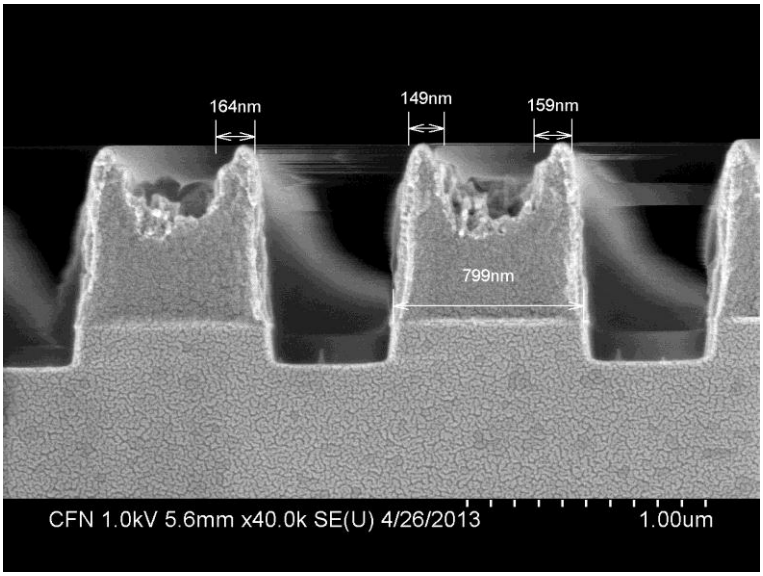

Figure 3.22 Cross section view of PMMA 6 cycle with 800 nm linewidth after 150 seconds SiO_2 etch

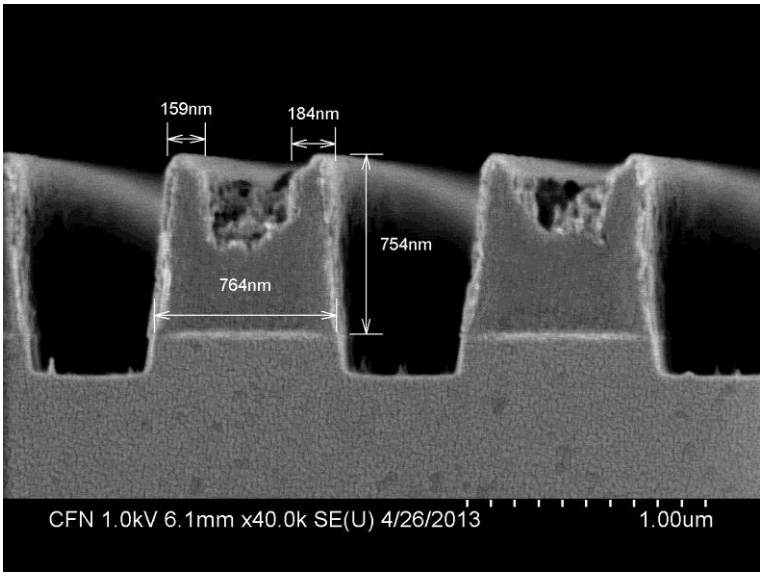

Figure 3.23 Cross section view of PMMA 9 cycle with 1 µm linewidth after 150 seconds SiO_2 etch

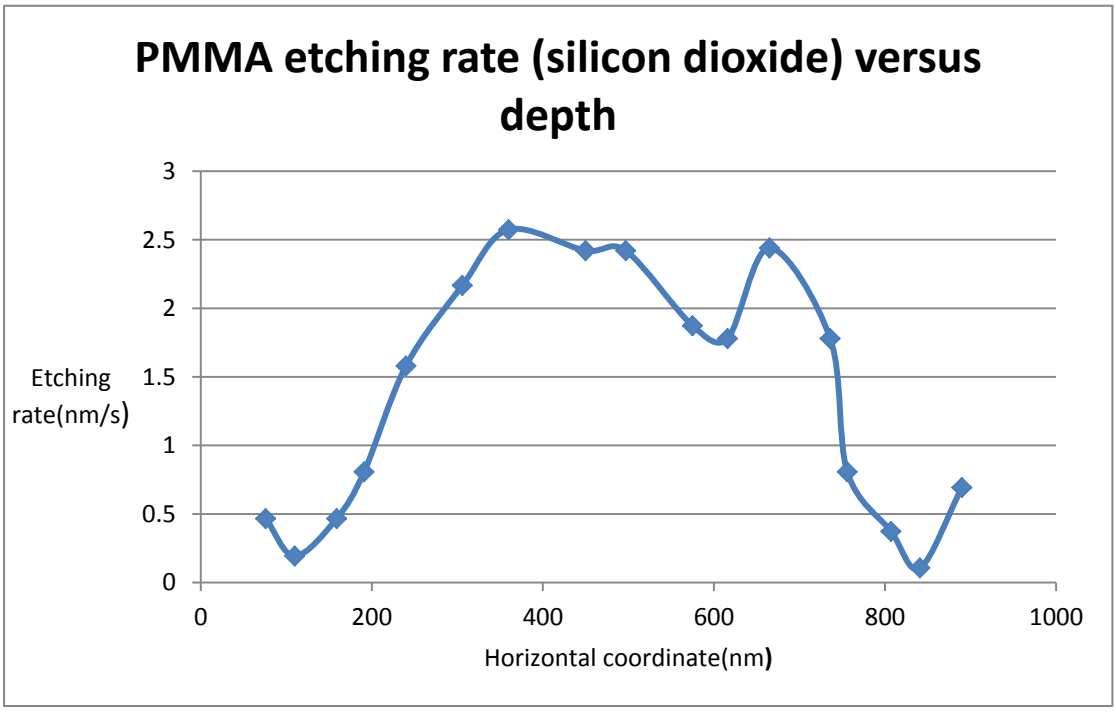

Figure 3.24 Etching rate (SiO_2) of PMMA with SIS 6 cycle versus depth

In Figure 3.24, the plot is not as smooth as that of O_2 etch and cryogenic silicon etch, and the slope is slower. Those effects are due to the high physical bombardment in the SiO_2 etch process, which obscures the effective depth surface.

3.5. Comments

By comparing the splitted parts in three etch recipes, the remaining heights with fully enhancement after etching are all around 750 nm without much variation along with different recipes and etching times. That appearance proves the high resistance of Al_2O_3 modified PMMA to various gases.

4. ZEP520 etching resistance analysis

4.1. Introduction to ZEP520

ZEP520 is a type of positive e-beam resist patented by Nippon Zeon Co. It was invented twenty years ago with a higher sensitivity and etch durability compared to conventional PMMA resist. ZEP520, of which the structure is shown in Figure 3.20, consists of a virtual 1:1 copolymer of α-chloromethacrylate and α-methylstyrene, which is dissolved in anisole. The α-Cl group provides a high sensitivity and the α-methylstyrene offers a high etching durability (etching resistance).[34]

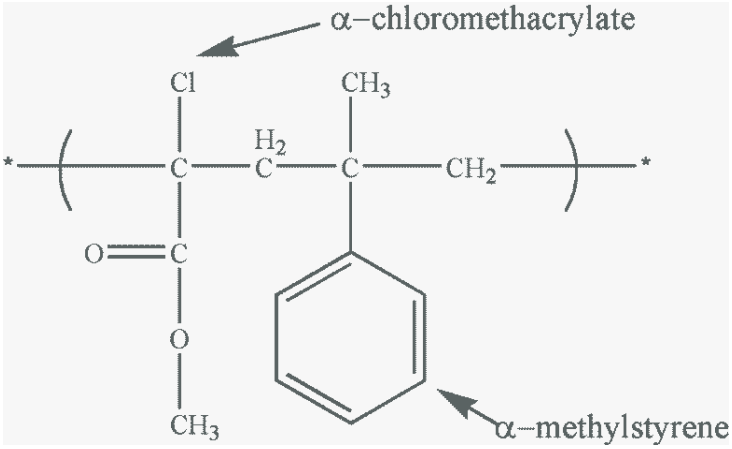

Figure 3.25 Chemical structure of ZEP520

4.2. ZEP520 etch profile after 50 seconds oxygen etch

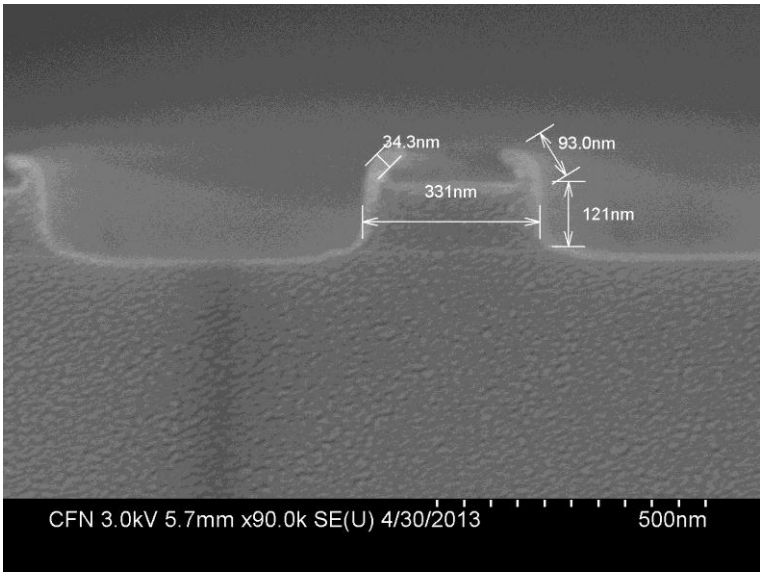

Figure 3.26 Cross section view of ZEP520 1 cycle after 50 seconds O_2 etch

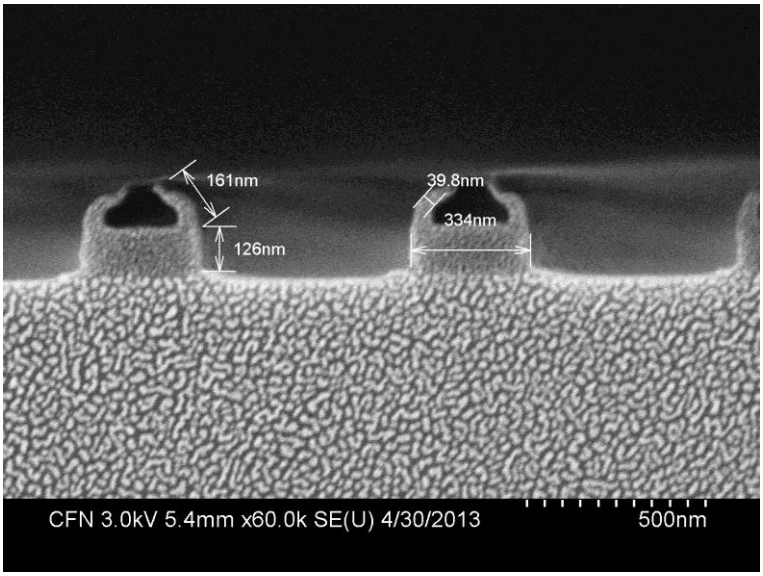

Figure 3.27 Cross section view of ZEP520 3 cycle after 50 seconds O_2 etch

From Figure 3.26 and Figure 3.27, it seems Al_2O_3 doesn't enhance the etching resistance very deep into ZEP520, only about 35 nm ~ 40 nm in the case of 1 cycle ALD, which is close to that for 3, 6, 9 cycles. The effective depth here is irrespective of the number of cycles. However, the modified resistance against oxygen plasma varies with ALD cycles, the heights of splitted peaks are respectively 93 nm in 1 cycle, 161 nm in 3 cycle, 226 nm in 6 cycle, 241 nm in 9 cycle.

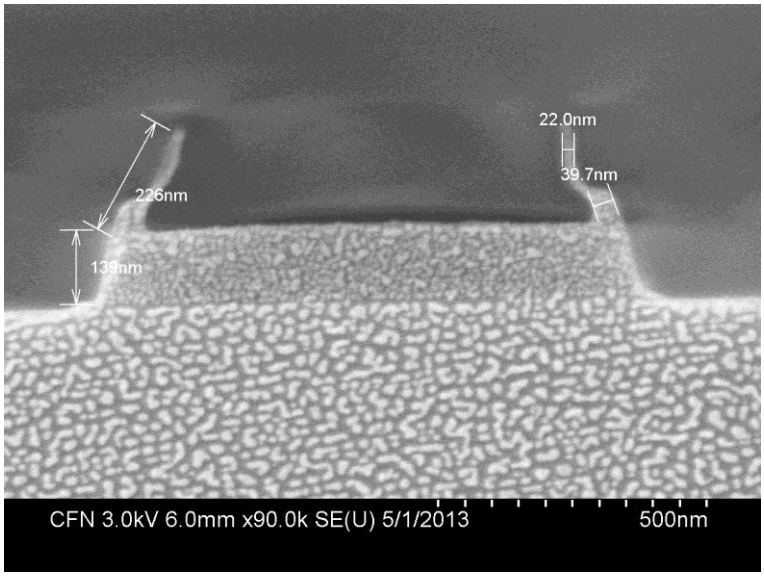

Figure 3.28 Cross section view of ZEP520 6 cycle after 50 seconds O_2 etch

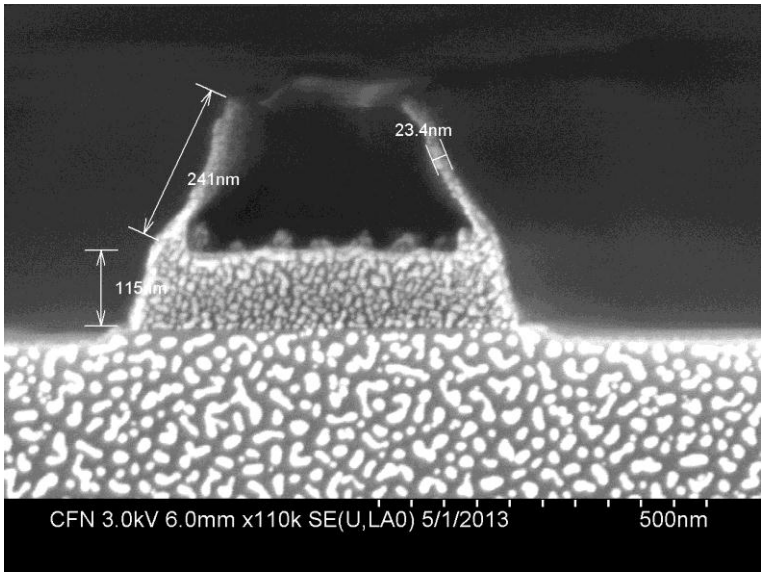

Figure 3.29 Cross section view of ZEP520 9 cycle after 50 seconds O_2 etch

4.3. ZEP520 etch profile after 45 seconds cryogenic etch

The effective depth in ZEP520 is so shallow that the thin cliff cannot survive in 1 cycle and 3 cycle ALD. In 6 cycle and 9 cycle, the consolidation effect intensifies, and a thin wall become observable but is too thin to be measured.

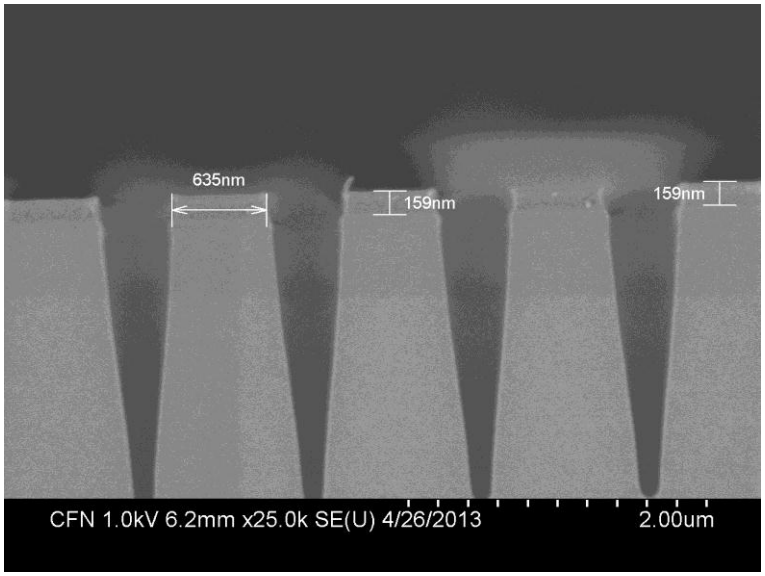

Figure 3.30 Cross section view of ZEP520 1 cycle after 45 seconds cryogenic silicon etch

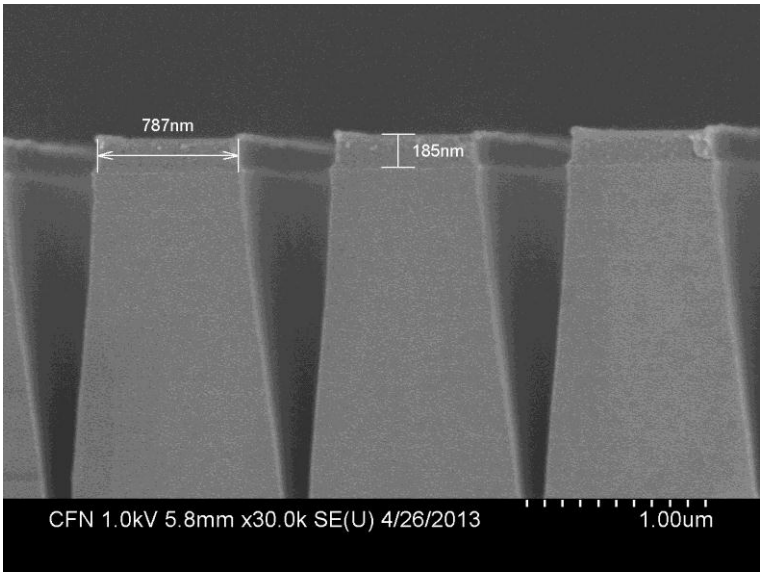

Figure 3.31 Cross section view of ZEP520 3 cycle after 45 seconds cryogenic silicon etch

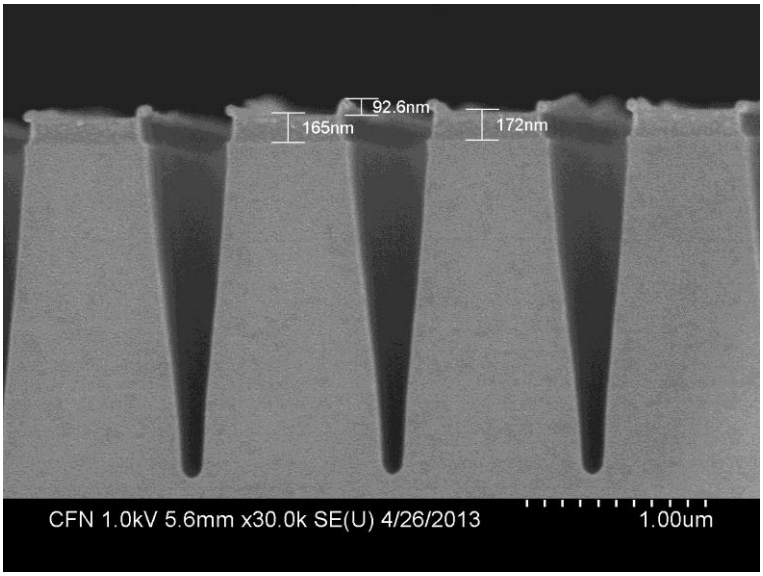

Figure 3.32 Cross section view of ZEP520 6 cycle after 45 seconds cryogenic silicon etch

Here we choose ZEP520 after 9 cycle ALD to analyze the etch resistance change by SIS process. The etch resistance against cryogenic silicon etch increases by a factor of 2.5.

	Original height (nm)	Height after etching (nm)	Etching time (s)	Etching rate (nm/s)
Untreated ZEP520	460	144	45	7
ZEP520 after SIS	460	332	45	2.8

Table 5 Comparison of silicon etching rate between 9 cycle SIS processed ZEP520 and unSIS processed ZEP520

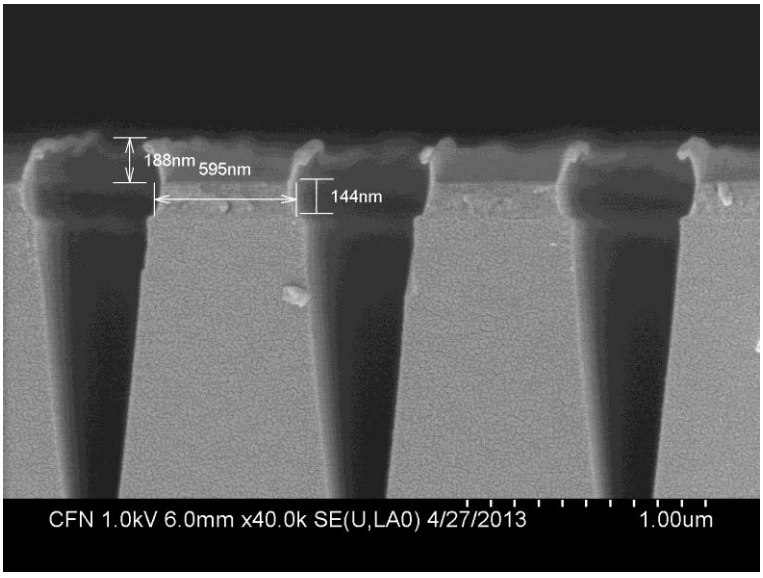

Figure 3.33 Cross section view of ZEP520 9 cycle after 45 seconds cryogenic silicon etch

4.4. ZEP520 etch profile after 50 seconds SiO_2 etch

SiO_2 etch recipe is fairly aggressive with a RF power of 40 W. SIS doesn't bring any obvious enhancement on ZEP520 against SiO_2 etch, the cross section view of 1 cycle sample shows no difference along horizontal direction.

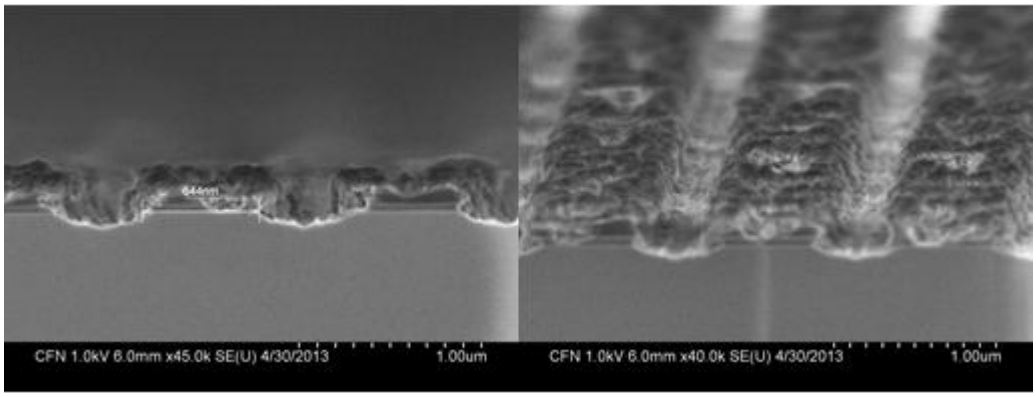

Figure 3.34 Cross section view of ZEP520 1 cycle after 50 seconds SiO_2 etch

For the later 3, 6, 9 cycle samples, the appearance is similar to that of 1 cycle. Considering the low effective depth observed in O_2 plasma etch and cryogenic silicon etch, the thin modified ZEP520 film does not preserve in this recipe.

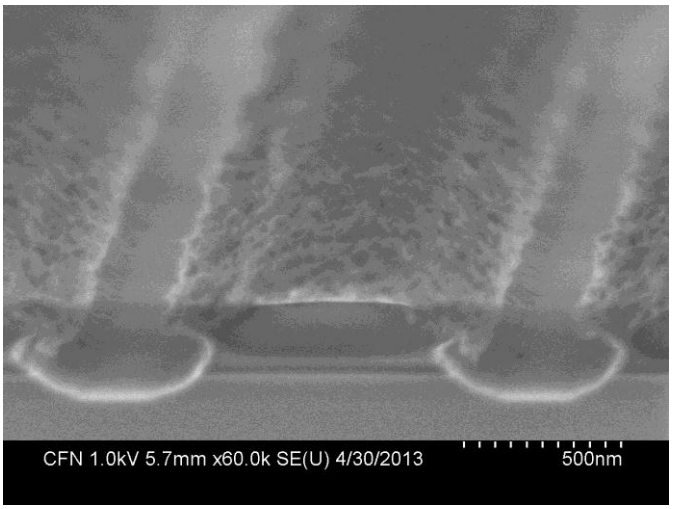

Figure 3.35 Cross section view of ZEP520 3 cycle after 50 seconds SiO_2 etch

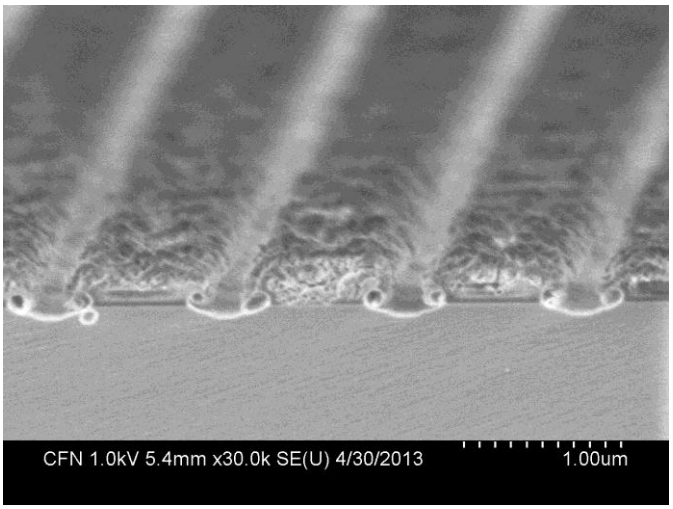

Figure 3.36 Cross section view of ZEP520 6 cycle after 50 seconds SiO_2 etch

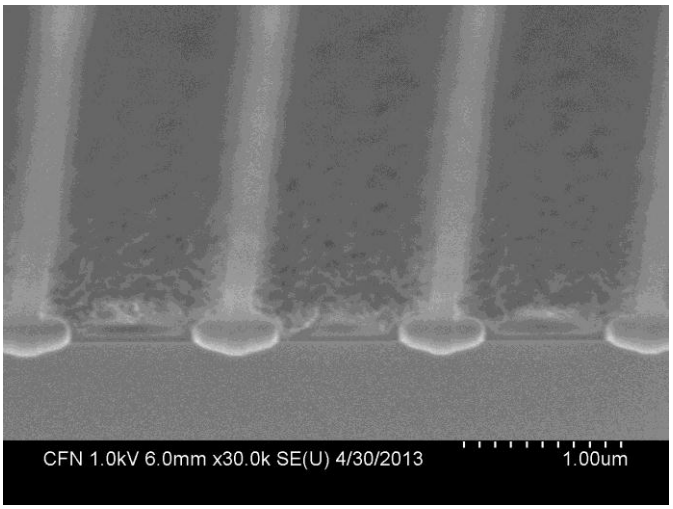

Figure 3.37 Cross section view of ZEP520 9 cycle after 50 seconds SiO_2 etch

5. S1811 etching resistance analysis

5.1. S1811 introduction

S1811 is a type of positive photoresist, which is sensitive to 365 nm i-line of mecury lamp light. The photoresists are composed of three basic components – resin, solvent, sensitizer and frequently have a fourth component of special additives.

The resin is an inert matrix of polymers which is used as binder to hold together the different materials in the resist and gives the resist its mechanical and chemical properties such as adhesion and chemical resistance. The resin in positive photoresist usually has a chemical structure of novolac shown in Figure 3.38. Solvent keeps the resist in its liquid state until it is applied to the wafer substrate. The resist sensitizer is the photosensitive component (PAC) of the resist material. In positive photoresist, it reacts in response to radiant energy in the form of light and acts to promote the

dissolution of resin in developer. The additives are used to control or modify specific chemical or light response aspects of resist material.

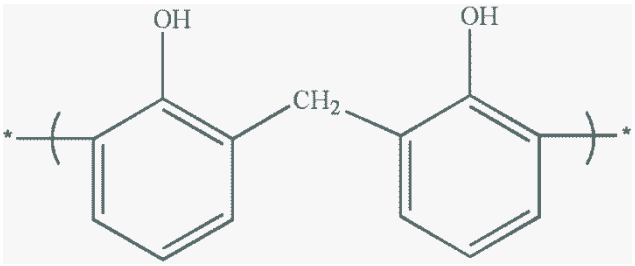

Figure 3.38 Novolac of S1811

5.2. S1811 etch profile after 75 seconds oxygen etch

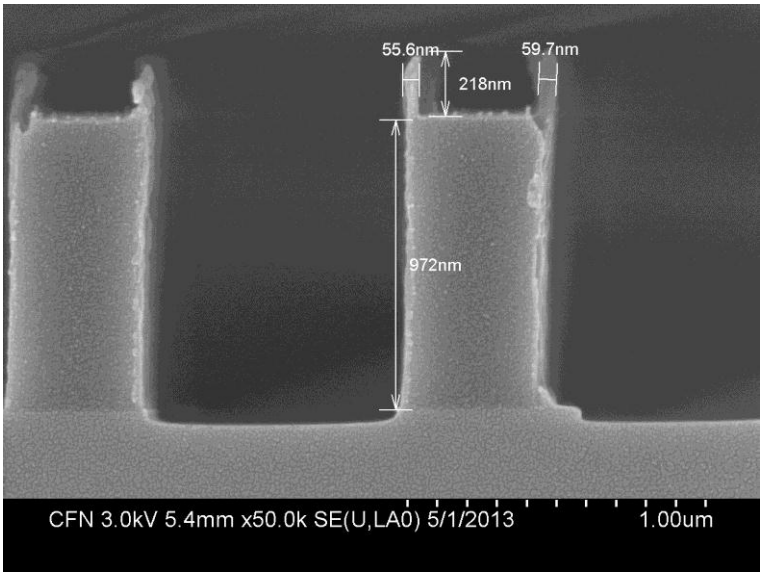

Figure 3.39 Cross section view of S1811 1 cycle after 75 seconds O_2 etch

From Figure 3.39 to Figure 3.42, we can see as the number of cycles increases, the effective depth increases slightly correspondingly, however the degree of enhancement doesn't improve successively along with the cycles, which is indicated by the difference in survived height after etching. For S1811, 3 cycle seems to be an upper limit of survived height, which doesn't increase with more SIS cycles.

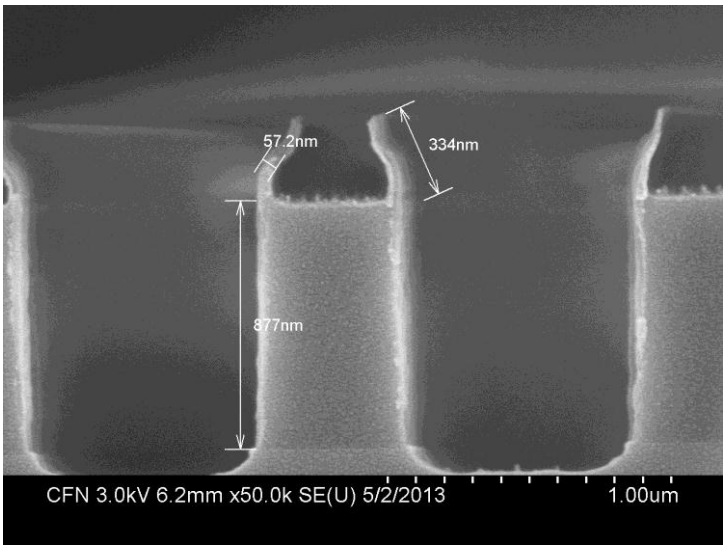

Figure 3.40 Cross section view of S1811 3 cycle after 75 seconds O_2 etch

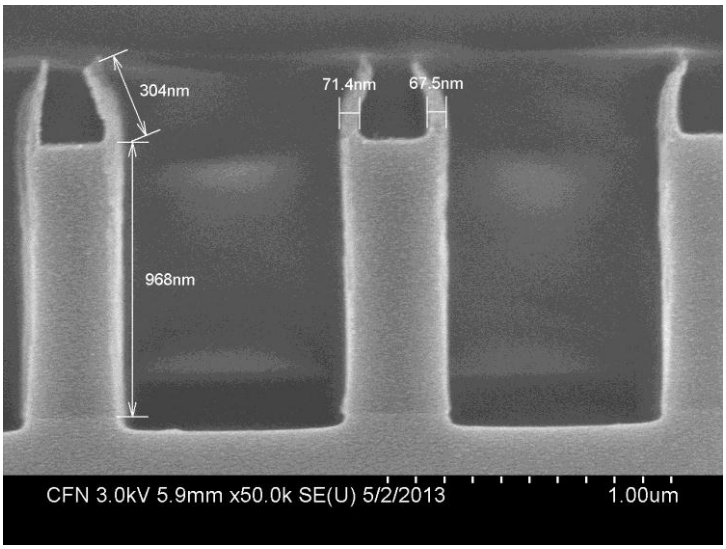

Figure 3.41 Cross section view of S1811 6 cycle after 75 seconds O_2 etch

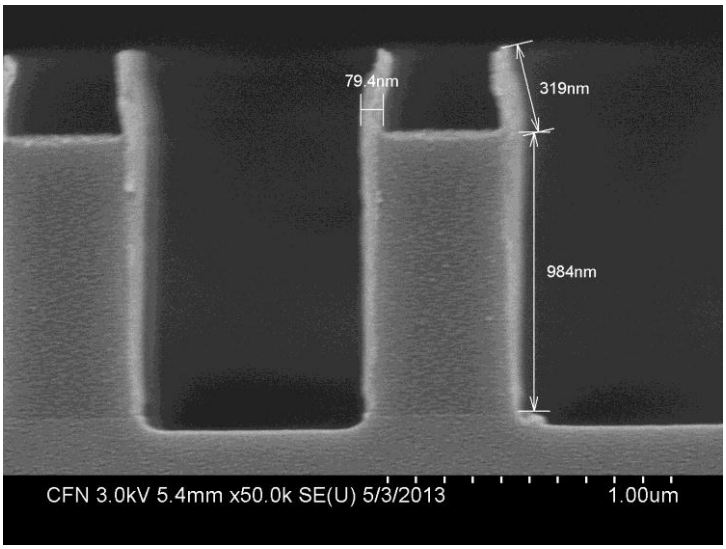

Figure 3.42 Cross section view of S1811 9 cycle after 75 seconds O_2 etch

From Figure 3.40, we can calculate that the etching resistance of S1811 against oxygen improves by a factor of 3.6, which remains unchanged regardless of SIS cycles.

	Original height (nm)	Height after etching (nm)	Etching time (s)	Etching rate (nm/s)
Untreated S1811	1340	877	75	6.2
SIS S1811	1340	1211	75	1.7

Table 6 Comparison of O_2 etching rate between 3 cycle SIS processed S1811 and unSIS processed S1811

A further study imposes SIS without a germanium barrier on the top surface and the resist is subjected to plasma etch. However, the result in Figure 3.43 shows the resistance increases along with the SIS cycles by measuring the remaining height after different time of etching. This result is contradictory to that obtained from cross sectional view images. The reason will be discussed in the next chapter.

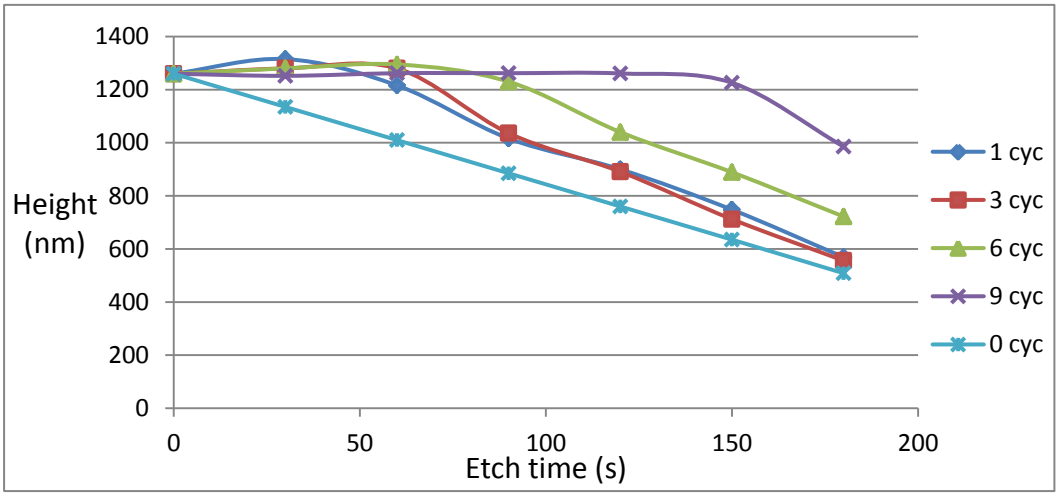

Figure 3.43 Height of remaining S1811 with different SIS cycles after O_2 etch

5.3. S1811 etch profile after 80 seconds cryogenic silicon etch

The effective depth which can withstand plasma in cryogenic silicon etch is slightly further than that in oxygen etch. With increase of the ALD cycles, two splitted edges perform a weird thickness change. The thicknesses are not uniform throughout the edges, the upper part tends to be thinner and the bottom part tends to be thicker. (Figure 3.44 – Figure 3.47)

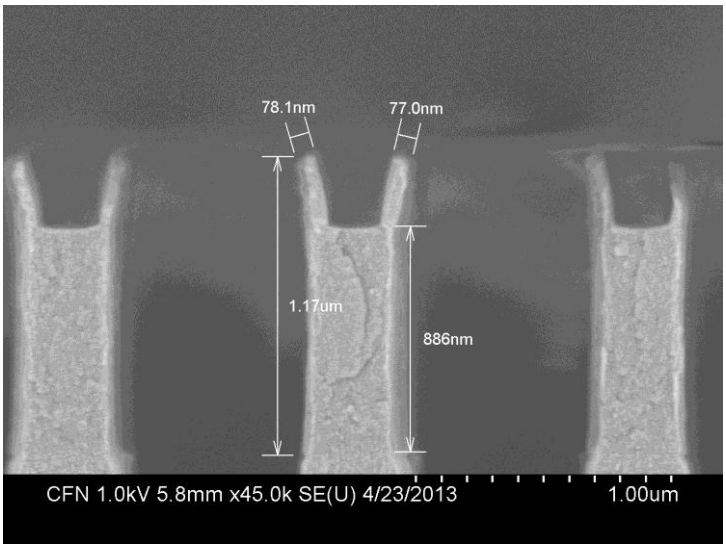

Figure 3.44 Cross section view of S1811 1 cycle after 80 seconds silicon etch

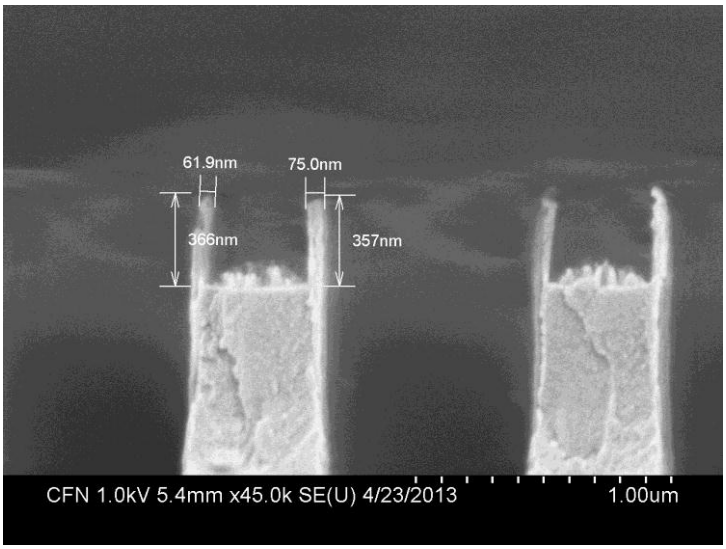

Figure 3.45 Cross section view of S1811 3 cycle after 80 seconds silicon etch

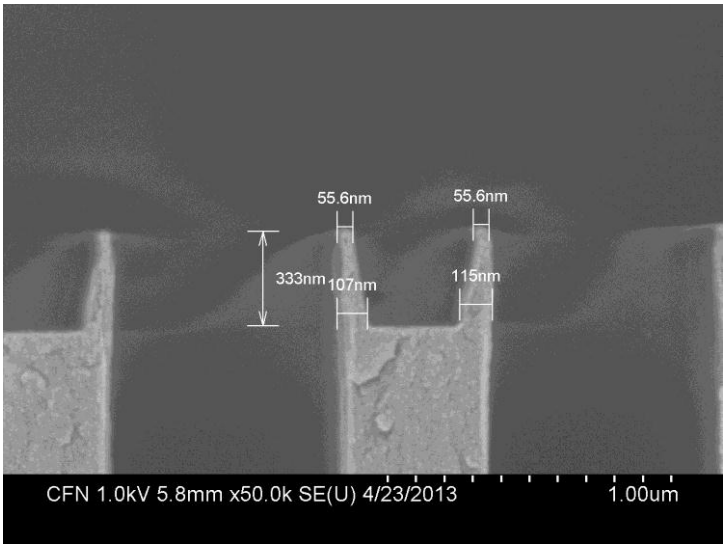

Figure 3.46 Cross section view of S1811 6 cycle after 80 seconds silicon etch

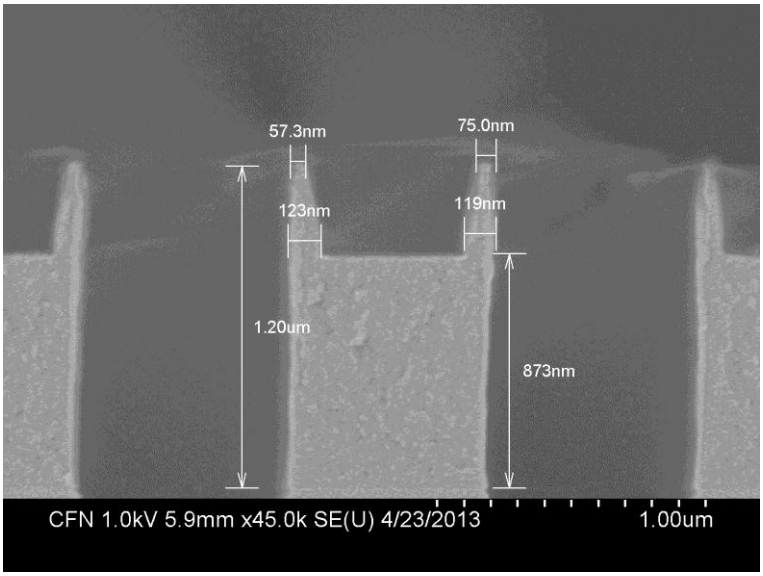

Figure 3.47 Cross section view of S1811 9 cycle after 80 seconds silicon etch

5.4. S1811 etch profile 105 seconds SiO_2 etch

The survived height of S1811 is 120 nm for the case of 1 cycle ALD as shown in Figure 3.48, and increases by ten nanometers for the case of more treatment cycle as shown from Figure 3.50. The effective depth is slightly increasing with the number of cycles as well as a sharper and clearer edge.

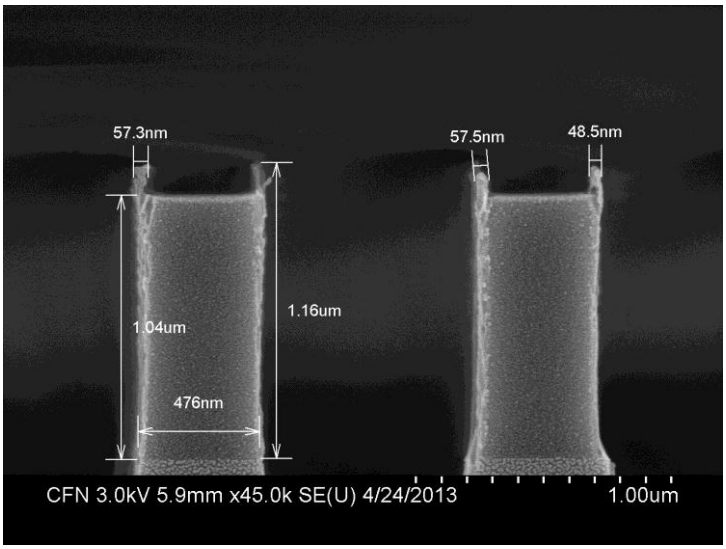

Figure 3.48 Cross section view of S1811 1 cycle after SiO_2 etch 105 seconds

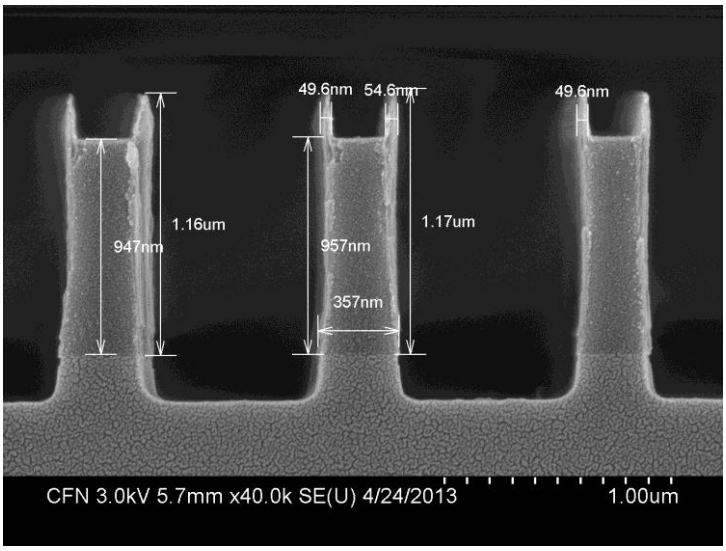

Figure 3.49 Cross section view of S1811 3 cycle after 105 seconds SiO_2 etch

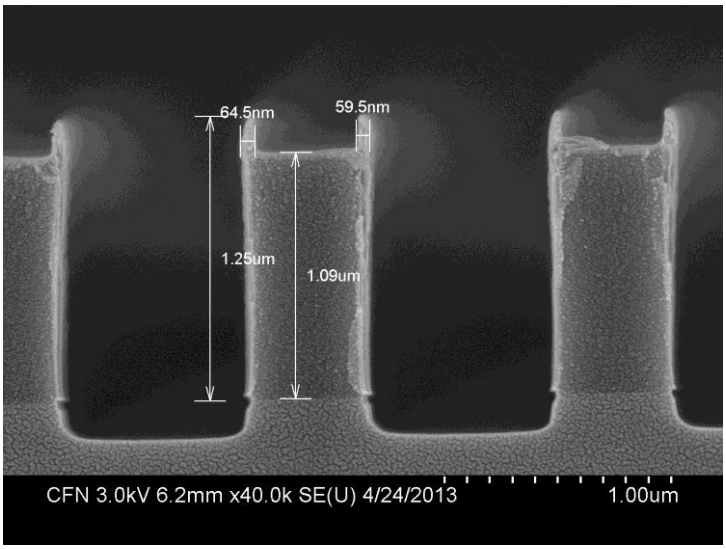

Figure 3.50 Cross section view of S1811 9 cycle after 105 seconds SiO_2 etch

6. ma-N 1410 etching resistance analysis

6.1. ma-N 1410 introduction

The ma-N 1410 resist is a negative novolac photoresist. It has the same component as positive novolac resist such as S1811. The main difference is that the PAC of negative resist will inhibit the dissolution of resin after exposure to light. The resin of ma-N 1410 is a specific phenolic resin with the novolac shown in Figure 3.51.

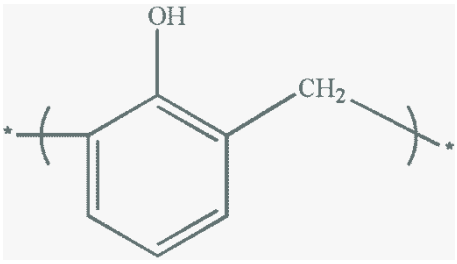

Figure 3.51 Novolac of ma-N 1410

6.2. ma-N 1410 etch profile after 45 seconds oxygen etch

In oxygen etch, ma-N 1410 performs similarly to S1811, with the only difference in a shallower effective depth, considering the fact that ma-N 1410 is negative resist, and becomes cross-linked after exposure, it may lead to a stronger interchain interaction in the polymer and therefore probably a larger resistance for the gaseous precursors in infiltrate inwards.

From Figure 3.52 and Figure 3.53, we can see the survived height is actually increasing with the SIS cycles from 1 to 3. After 3 cycle ALD, the survived height appears a weird decrease for the case of 9 cycle as shown in Figure 3.54 compared to 1 cycle and 3cycle SIS treated samples. That is probably due to the experimental error.

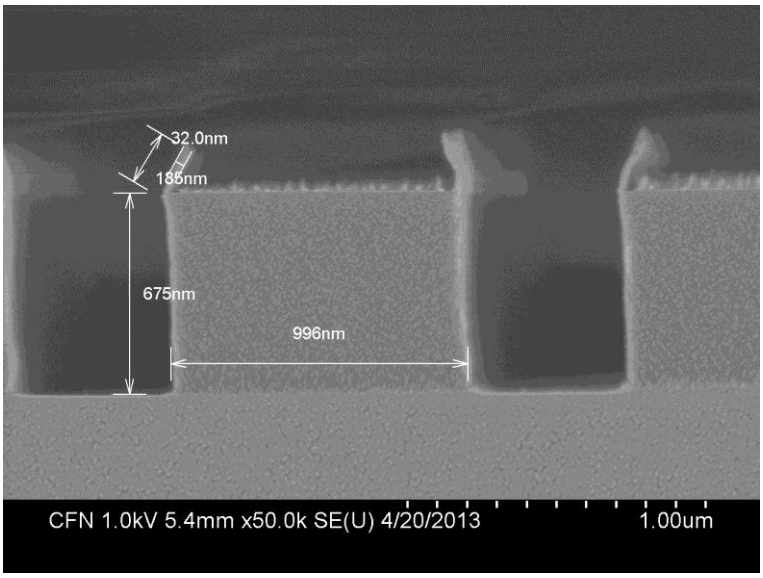

Figure 3.52 Cross section view of ma-N 1410 1 cycle after 45 seconds oxygen etch

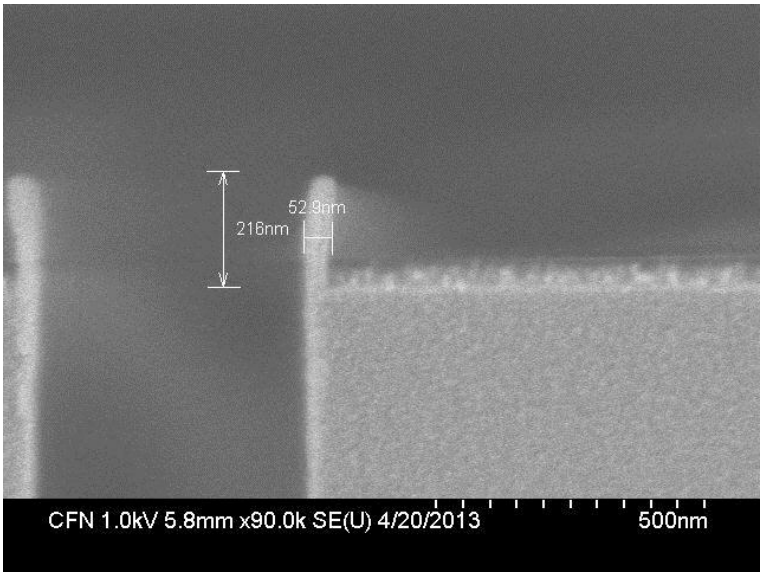

Figure 3.53 Cross section view of ma-N 1410 6 cycle after 45 seconds oxygen etch

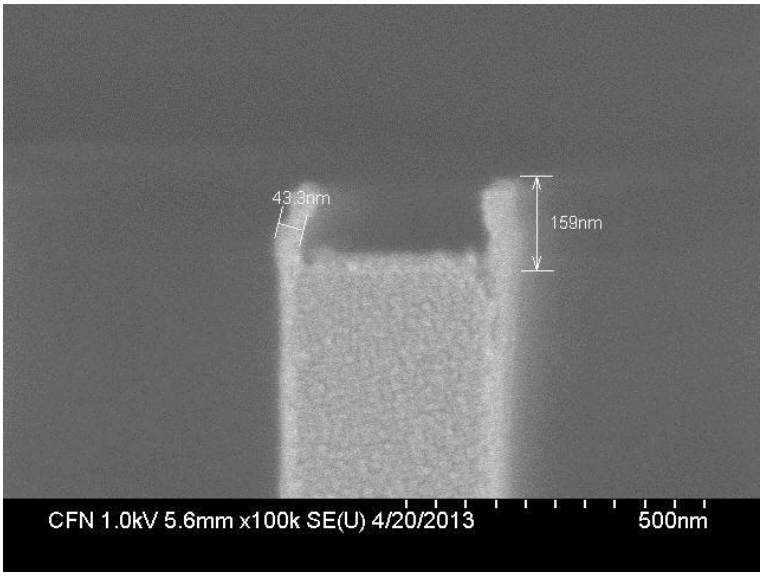

Figure 3.54 Cross section view of ma-N 1410 9 cycle after 45 seconds oxygen etch

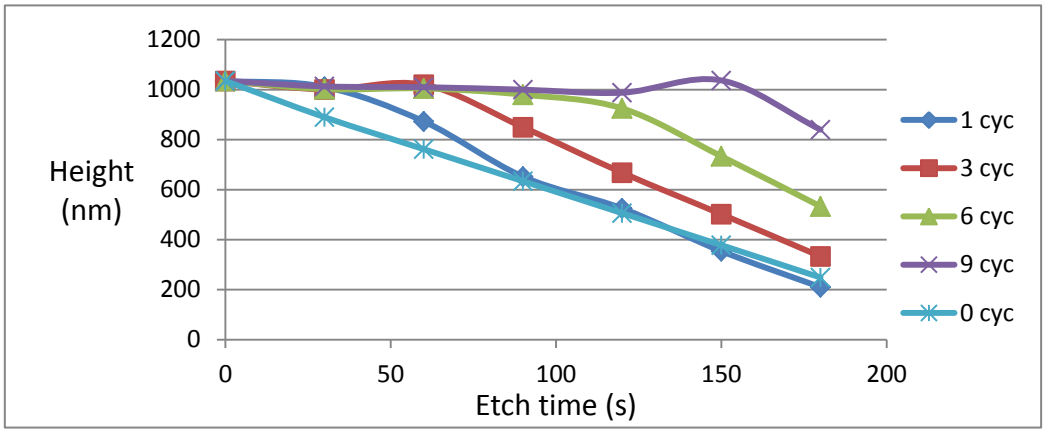

Figure 3.55 Height of remaining ma-N 1410 with different SIS cycles after O_2 etch

A similar study is carried out for ma-N 1410 as for S1811, and a similar plot is obtained as shown in Figure 3.55, which corresponds to the analysis in the next chapter.

6.3. ma-N 1410 etch profile after 70 seconds cryogenic silicon etch

ma-N 1410 with 1 cycle ALD barely performs any resistance to cryogenic silicon etch as shown in Figure 3.56. Even though increasing from 1 cycle to 3 cycle slightly increases the effective depth as shown in Figure 3.56 and Figure 3.57, the profile after etching improves apparently. By comparing 3 cycle with more ALD cycles, the resistance doesn't change much. The only difference that the splitted peaks is the more vertical, which may not affect properties in application, because in practical use the top surface will be treated by ALD as well, no splitted peaks will appear in that case.

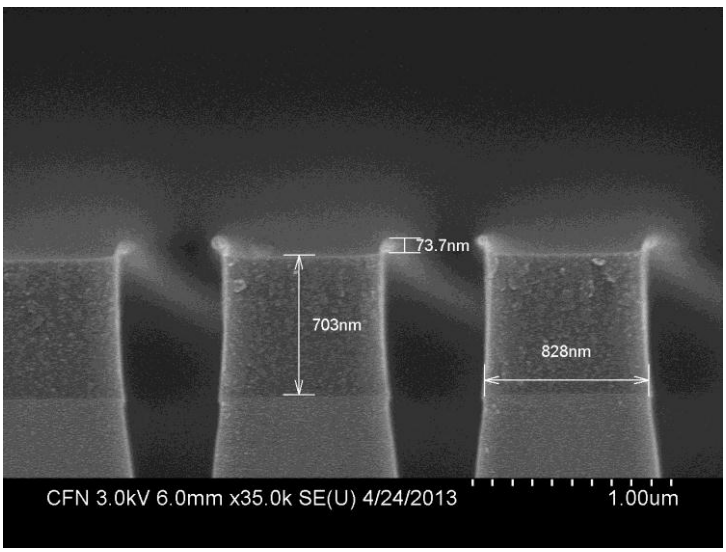

Figure 3.56 Cross section view of ma-N 1410 1 cycle after 70 seconds silicon etch

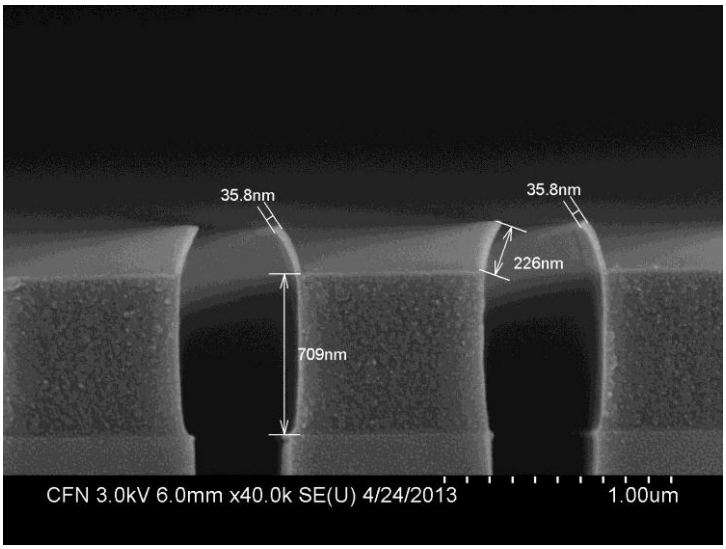

Figure 3.57 Cross section view of ma-N 1410 3 cycle after 70 seconds silicon etch

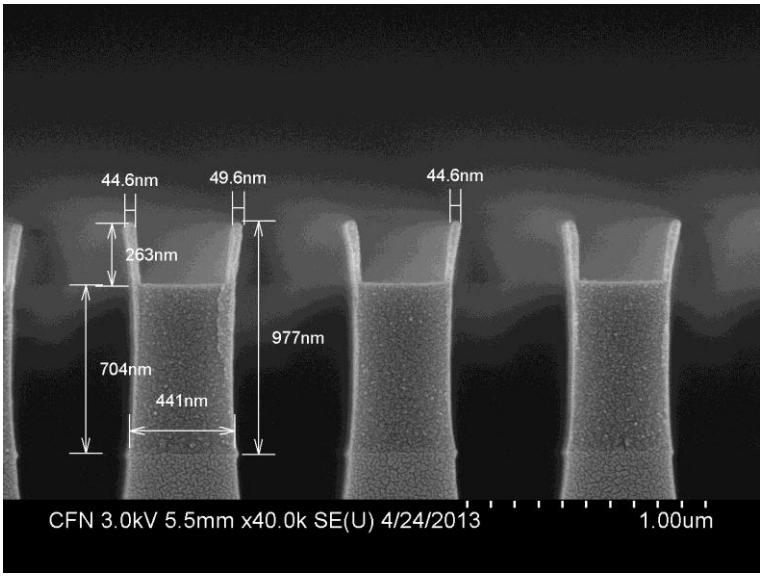

Figure 3.58 Cross section view of ma-N 1410 6 cycle after 70 seconds silicon etch

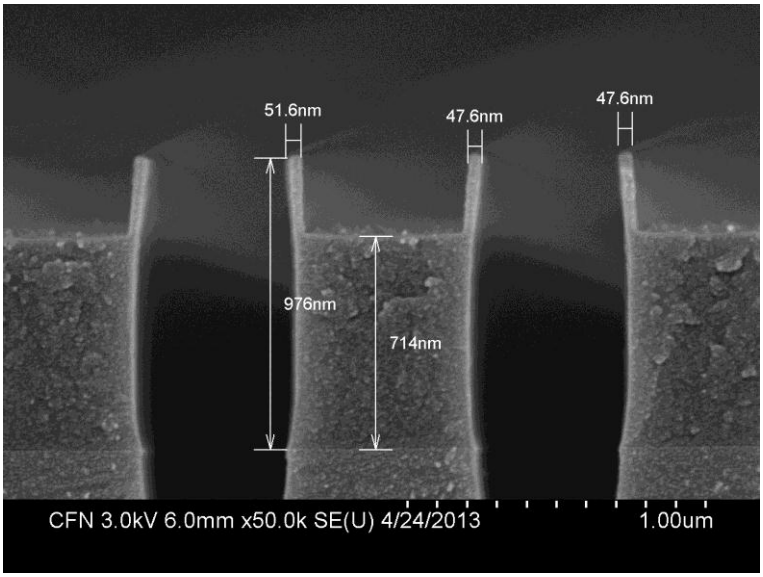

Figure 3.59 Cross section view of ma-N 1410 9 cycle after 70 seconds silicon etch

6.4. ma-N 1410 etch profile after 150 seconds SiO_2 etch

ma-N 1410 with 1 cycle treatment barely perform any resistance to SiO_2 etch process as shown in Figure 3.60, while increasing the SIS cycles from 1 to 3, visible improvement is observed in Figure 3.61, but no more enhancement occurs after 3 cycle.

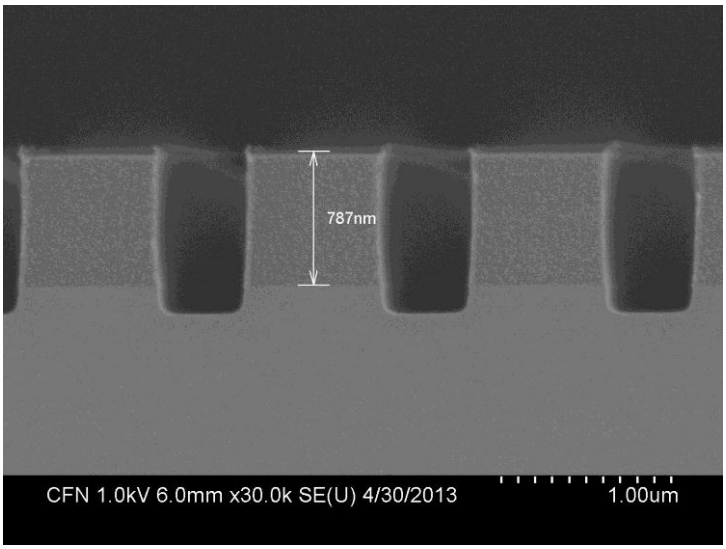

Figure 3.60 Cross section view of ma-N 1410 1 cycle after 150 seconds SiO_2 etch

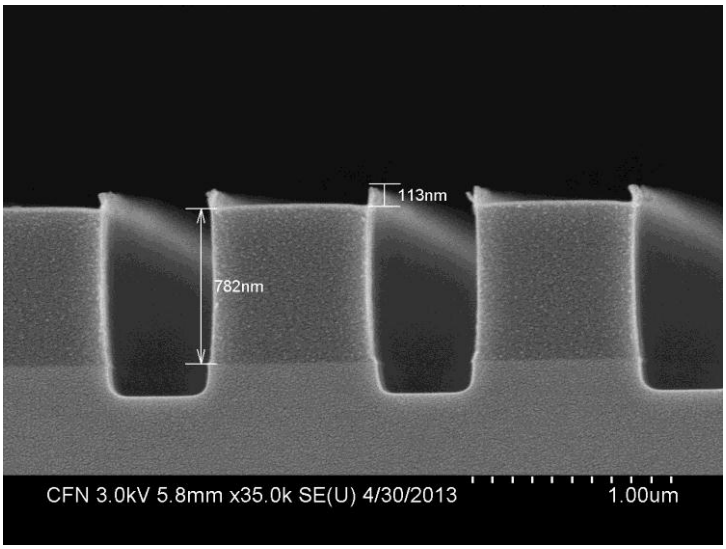

Figure 3.61 Cross section view of ma-N 1410 3 cycle after 150 seconds SiO_2 etch

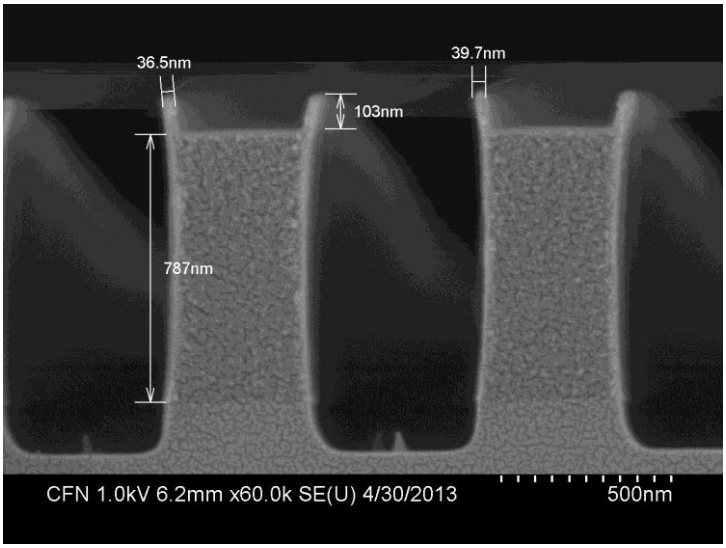

Figure 3.62 Cross section view of ma-N 1410 6 cycle after 150 seconds SiO_2 etch

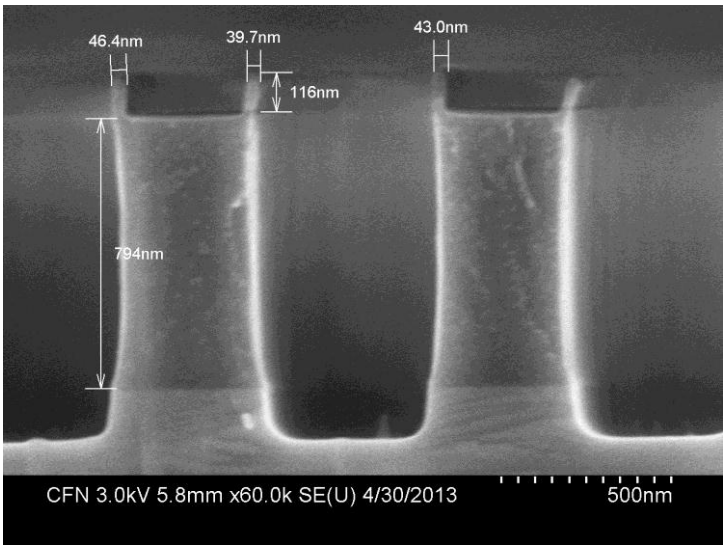

Figure 3.63 Cross section view of ma-N 1410 9 cycle after 150 seconds SiO_2 etch

Chapter IV Analysis on modification degree and infiltration depth

1. Infiltration mechanism

From the SEM images, we can come to the conclusion that the properties of all the four types of resist against different etch processes have been modified to different extent except for ZEP520 against SiO_2 etch. The effective depths also vary among different types of resists.

For PMMA, since the etching profiles of different SIS cycles treated samples are similar and don't have much difference in effective depth, we can conclude that the later SIS treatments don't play a role in the resistance enhancement. For S1811 and ma-N 1410, the results of direct deposition method as shown in Figure 3.43 and Figure 3.55 shows that without a barrier layer on the surface of resist, the resistance performs a visible increase along with more SIS treatment.

What has to be clarified before the infiltration mechanism is that effective depth observed in SEM images is not exactly equal to infiltration depth of precursors. They are correlated but not the same. There might be an enhancement threshold beyond which the SIS enhanced resist would withstand plasma etch. The following mechanism is based on that effective depth and infiltration depth are positive correlated.

From the effects above, we conclude that the precursors diffuse into the bulk of resist only in the first few cycles of SIS. The Al_2O_3 formed near the surface will hinder the precursors in latter cycles to infiltrate, leading to direct deposition of Al_2O_3 on the surface with thickness increasing with SIS cycles. That explains the low improving factor and uncorrelation to SIS cycles in the cross section method, since the thin Al_2O_3 film only locates on the sidewall surface. The thin film can survive in the later plasma etching process, however due to its thin thickness (should be less than 1 nm), the film may collapse, even though it doesn't collapse, it is unobservable under SEM.

2. Diffusion depth analysis based on resist chemical structures

As stated before, the photoresists are composed of three basic components – resin, solvent, sensitizer and frequently have a fourth component of special additives.

The resin is an inert matrix of polymers which is used as binder to hold together the different materials in the resist and gives the resist its mechanical and chemical properties such as adhesion and chemical resistance.

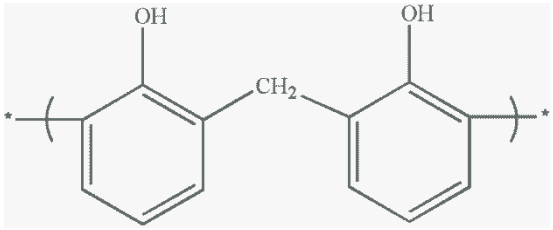

Figure 4.1 Novolac of S1811

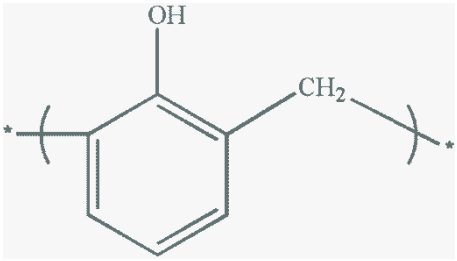

Figure 4.2 Novolac of ma-N 1410

The resin of PMMA and ZEP520 themselves are photosensitive. PMMA is a synthetic resin produced from polymerization of methyl methacrylate.

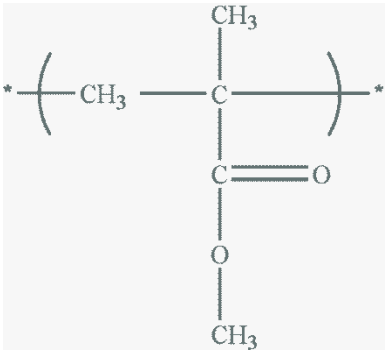

Figure 4.3 Chemical structure of PMMA

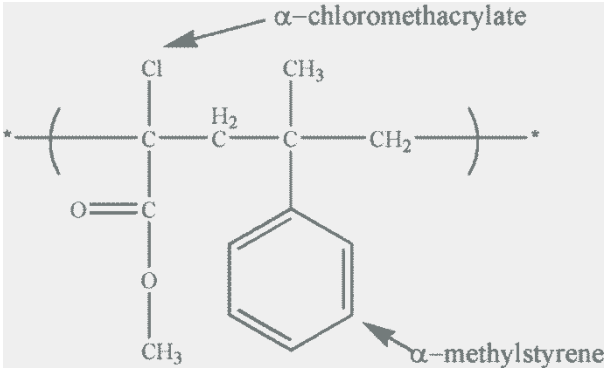

Figure 4.4 Chemical structure of ZEP520

From the chemical structures of the four resists along with effective depth measurement, we find that resists with benzene rings in their structures (S1811, ma-N 1410, ZEP520) tend to have shallow diffusion depths of precursors during SIS, while resist without benzene rings (PMMA) is deeply enhanced. We suspect that benzene rings have an intense influence on restraining diffusion.

Chapter V Conclusion

In our research, the plasma etch resistance of four typical resist was successfully improved by sequential infiltration synthesis. By designing a germanium layer to block the infiltration from the top, we were able to observe etching profile along infiltration direction, and from that study the infiltration depth and the degree of resistance enhancement degree in different etch recipes.

Photoresist S1811 and ma-N 1410 had similar etch profiles due to their similar component and chemical structures. 3 cycles of SIS could provide sufficient resistance improvement, the number of SIS cycles only changed infiltration depth slightly.

PMMA and ZEP520, even though were both e-beam resist, had completely disparate etch profiles. ZEP520 which had benzene rings in its chemical structure like S1811 and ma-N 1410, had similar modification, but with a shallower effective diffusion depth than those two photoresist. Without any benzene rings, PMMA can be deeply infiltrated by precursors in the first cycle of SIS.

The infiltration mechanism and influencing factor were proposed. The infiltration only occurred in the first few cycles of ALD, the Al_2O_3 formed would block later precursors to infiltrate, leading to direct deposition on the surface. The infiltration depth could be related to the benzene rings in the chemical structure, which still need more research to confirm.

Even though the infiltrating depth is shallow in some resist materials, and may not modify the whole bulk of resist, we can conduct SIS and etching process alternately, which provides a promising method to achieve deep etch in industry.

Reference

[1] M. Qurik, J. Serda, *Semiconductor Manufacturing Technology*. Prentice Hall, **2000**.
[2] M. Shearn, X. Sun, M. D. Henry, *Advanced Plasma Processing: Etching, Deposition, and Wafer Bonding Techniques for Semiconductor Applications, Semiconductor Technologies*. InTech, **2010**.
[3] M. Qurik and J. Serda, *Semiconductor Manufacturing Technology*. Prentice Hall, **2000**.
[4] M. J. Walker, *Proc. SPIE Int. Soc. Opt. Eng* **2001**, 4407, 89.
[5] International Technology Roadmap for semiconductors, http://www.itrs.net.
[6] Y. C. Tseng, A. U. Mane, J. W. Elam, S. B. Darling, *Adv. Mater*. **2012**, 24, 2608.
[7] D. F. Kyser, *J. Vac. Sci. Technol., B* **1983**, 1, 1391.
[8] A. N. Broers, A. C. F. Hoole, J. M. Ryan, *Microelectronic Engineering* **1996**, 32, 131.
[9] K. W. Lee, S. M. Yoon, S. C. Lee, W. Lee, I. M. Kim, C. E. Lee, *J. Kor. Phys. Soc.* **2009**, 55, 1720.
[10] H. K. Qian, W. Zhou, J. Miao, L. E. Lim and X. R. Zeng, *J. Micromech. Microeng*., **2008**, 18.
[11] M. D. Henry, M. J. Shearn, B. Chhim, A. Scherer, *Nanotechnology*, **2010,** 21, 245.
[12] V. B. Aleskovskii, Zh. Prikl. Khim, *J. Appl. Chem. USSR*, **1974**, 47, 2145.
[13] George, S. M. Atomic Layer Deposition: An overview *Chem. Rev.* **2010,** 110, 111-131
[14] M. H. Somervell, D. S. Fryer, B. Osborn, K. Patterson, J. Byers, and C. G. Willson, *J. Vac. Sco. Technol. B* **2000**, 18, 2551.
[15] F. Coopmans and B. Roland, *Solid State Technol* **1987**, 30, 93.
[16] E. K. Pavelchek, J. F. Boland, J. W. Thackeray, G. W. Orsular, S. K. Jones, B. W. Dudley, S. M. Bobbio, and P. W. Freeman, *J. Vac. Sci. Technol*. B **1990**, 8, 1497.
[17] S. Tedesco, C. Pierrat, F. Vinet, B. Florin, M. Lerme, and J. C. Guibert, *Proc. SPIE Int. Soc. Opt. Eng* **1990**, 1263, 282.
[18] A. Sinha, Dennis. H. Hess, and C. L. Hendreson, *Electrochemical and Solid-State Letters* **2006**, 9, (11) G330-G333.
[19] Yu-Chih. Tseng, Q. Peng, L. E. Ocola, J. W. Elam, and S. B. Darling, *J. Phys. Chem*. C **2011**, 115, 17725.
[20] Q. Peng, Y. C. Tseng, S. B. Darling, J. W. Elam, *ACS Nano* **2011**, 5, 4600.
[21] Q. Peng, Y. C. Tseng, S. B. Darling, J. W. Elam, *Adv. Matter.* **2010**, 22, 5129.
[22] C. J. Hawker, T. P. Russell, *MRS Bull*. **2005**, 30, 952.
[23] J. Y. Cheng, A. M. Mayers, C. A. Ross, *Nat. Mater*. **2004**, 3, 823.
[24] R. Ruiz, H. M. Kang, F. A. Detcheverry, E. Dobisz, D. S. Kercher, T. R. Albrecht, J. J. de Pablo, P. F. Nealey, *Science* **2008**, 321, 936.
[25] S. B. Darling, *Prog. Polym. Sci*. **2007**, 32, 1152.
[26] J. Y. Cheng, C. A. Ross, V. Z. H. Chan, E. L. Thomas, R. G. H. Lammertink, G. J. Vancso, *Adv. Mater*. **2001**, 13, 1174.

[27] C. T. Black, K. W. Guarini, K. R. Milkove, S. M. Baker, T. P. Russell, M. T. Tuominen, *Appl. Phys. Lett*. **2001**, 79, 409.
[28] C. T. Black, R. Ruiz, G. Breyta, J. Y. Cheng, M. E. Colburn, K. W. Guarini, H. C. Kim, Y. Zhang, *IBM J. Res. Dev*. **2007**, 51, 605.
[29] G. L. Liu, C. S. Thomas, G. S. W. Graig, P. F. Nealey, *Adv. Funct. Mater*. **2010**, 20, 1251.
[30] M. J. Fasolka, A. M. Mayes, *Annu. Rev. Mater. Res*. **2001**, 31, 323.
[31] J. Bang, U. Jeong, D. Y. Ryu, T. P. Russell, C. J. Hawker, *Adv. Mater*. **2009**, 21, 4769
[32] H. C. Kim, S. M. Park, W. D. Hinsberg, *Chem. Rev*. **2010**, 110, 146.
[33] N. R. Rueger, J. J. Beulens, M. Schaepkens, M. F. Doemling, J. M. Mirza, T. E. F. M. Standaert and G. S. Oehrlein, *J. Vac. Sci. Technol. A*. **1997**, 15.1881.
[34] T. Nishida, M. Notomi, R. Iga, T. Tamamura, *Jpn. J. Appl. Phys*. **1992**, 31, 4508.